AD-759 917

DYNAMIC FRACTURE CRITERIA FOR POLYCARBONATE AND POLYIMIDE

Stanford Research Institute

Prepared for:

Ballistic Research Laboratories

March 1973

BRL CR 91

AD 759917

BRL

AD

CONTRACT REPORT NO. 91

DYNAMIC FRACTURE CRITERIA FOR POLYCARBONATE AND POLYIMIDE

Prepared by

Stanford Research Institute
333 Ravenswood Avenue
Menlo Park, California

March 1973

USA BALLISTIC RESEARCH LABORATORIES
ABERDEEN PROVING GROUND, MARYLAND

94

CONTRACT REPORT NO. 91

Final Report

MARCH 1973

DYNAMIC FRACTURE CRITERIA FOR POLYCARBONATE AND POLYIMIDE

By: D. R. CURRAN and D. A. SHOCKEY

Prepared for:

BALLISTIC RESEARCH LABORATORY
ABERDEEN PROVING GROUND
ABERDEEN, MARYLAND 21005

CONTRACT DAAD05-71-C-0180

SRI Project 1033

Approved by:

G. R. ABRAHAMSON, *Director*
Poulter Laboratory

C. J. COOK, *Executive Director*
Physical Sciences Division

Unclassified
Security Classification

DOCUMENT CONTROL DATA - R & D

(Security classification of title, body of abstract and indexing annotation must be entered when the overall report is classified)

1. ORIGINATING ACTIVITY *(Corporate author)* Stanford Research Institute 333 Ravenswood Avenue Menlo Park, California	2a. REPORT SECURITY CLASSIFICATION Unclassified 2b. GROUP

3. REPORT TITLE

Dynamic Fracture Criteria for Polycarbonate and Polyimide

4. DESCRIPTIVE NOTES *(Type of report and inclusive dates)*

5. AUTHOR(S) *(First name, middle initial, last name)*

D. R. Curran & D. A. Shockey

6. REPORT DATE MARCH 1973	7a. TOTAL NO. OF PAGES 94	7b. NO. OF REFS
8a. CONTRACT OR GRANT NO. DAAD05-71-C-0180 b. PROJECT NO. 5025.11.29700 c. d.	9a. ORIGINATOR'S REPORT NUMBER(S) BRL CONTRACT REPORT NO. 91 9b. OTHER REPORT NO(S) *(Any other numbers that may be assigned this report)*	

10. DISTRIBUTION STATEMENT

Approved for public release; distribution unlimited.

11. SUPPLEMENTARY NOTES	12. SPONSORING MILITARY ACTIVITY U.S. Army Ballistic Research Laboratories Aberdeen Proving Ground, Maryland 21005

13. ABSTRACT

This report describes the results of a study of the dynamic fracture characteristics of polymers. The main objective of the study was to develop the capability to predict quantitatively the level of damage produced in polymeric materials under known dynamic loads. To accomplish this objective, disk-shaped specimens of polycarbonate, a relatively tough polymer, and polyimide, a brittle high temperature polymer, were subjected to flat-plate impact in a light gas gun under well-controlled and well-monitored conditions. For polycarbonate the stress-volume loading and unloading paths were determined under both static and dynamic conditions. Quantitative fractographic analyses on the impacted polycarbonate specimens were carried out and the results were correlated with computed stress histories to obtain analytical relations and graphs enabling one to predict the extent of damage which will be produced in polycarbonate by an arbitrary dynamic load. A similar detailed analysis was not carried out for polyimide because this brittle material fractured in a much more catastrophic manner; for a given stress duration a small stress increment covered the range from incipient shock damage to complete disintegration. However, static stress-volume loading and unloading curves, an approximate constitutive relation, and the shock damage threshold stress for stress durations of about a microsecond were obtained for polyimide. A detailed study of the fracture mechanism was made for both materials.

DD FORM 1 NOV 65 1473 REPLACES DD FORM 1473, 1 JAN 64, WHICH IS OBSOLETE FOR ARMY USE.

Unclassified
Security Classification

Preceding page blank

CONTENTS

LIST OF FIGURES

Preceding page blank

LIST OF TABLES

Preceding page blank

I INTRODUCTION

Shock damage in solids is caused by short-lived tensile pulses resulting from the intersection of reflected shock waves. Dynamic loads of this type result from high velocity impact, close proximity to detonating high explosive, and short term radiation deposition. The last case is of particular interest for heat shield materials. Such materials often consist of strong fibers in a polymer matrix and are more complex than monolithic materials. Thus, the task of characterizing their resistance to shock damage is correspondingly more formidable. The problems involved can often be reduced by solving the lesser problems associated with the characterization of the component materials.

During the last two years, a new approach to the shock damage problem has been developed and fully documented at SRI.[1,2] This approach utilizes flat-plate impact experiments similar to those of previous workers to produce shock damage, but the microscopic damage characterization and stress history determination are performed with much greater sophistication. Quantitative damage nucleation and growth rate functions $\dot{N}$ and $\dot{R}$ are obtained which are considered to be material properties that characterize susceptibility to shock damage. These functions are expected to be independent of the loading source and may thus describe damage resulting from impact, from radiation deposition, or from any other dynamic loading mechanism. This approach, hereafter referred to as the NAG (nucleation and growth) approach, was used in the current project to obtain quantitative data for polycarbonate and polyimide polymers.

Preceding page blank

II MATERIALS AND EXPERIMENTS

Selection of Materials

The variation of mechanical properties within the class of materials known as polymers is considerable and results from the seemingly countless permutations of chemical and molecular structure, degree of crystallinity, degree of crosslinking, macroscopic texture, and the influences of thermal-mechanical treatments and fabrication procedures.

Of particular interest in this work is the wide range that exists in toughnesses and thermal properties. Since testing materials at opposite ends of the toughness spectrum provides the maximum opportunity to study the behavior of polymers as a class of materials, a tough and a brittle polymer under quasi-static loading at room temperature were chosen for investigation.

For the tough polymer, a transparent polycarbonate resin developed by the General Electric Company and marketed under the trade name of Lexan was selected. Its high impact strength in small sections greatly exceeds that of other engineering grade thermoplastics and, coupled with its above average high-temperature properties, leads to its application in housings for power tools and electrical connectors, pressure vessels, gears, and shotgun shells.

Results of the standard Izod toughness tests show that polycarbonate is up to 10 times tougher than other polymers in small sections. For sections greater than about 0.14 to 0.16 in. on a side, however, toughness drops to a minimal value and fracture occurs in a brittle fashion. Also a time-temperature-transition curve for a 1/8 in. Izod specimen shows a drop in impact strength from about 14 to 16 ft lb/in. of notch to 2 to 3 at about 0^{o}F (Figure 1).

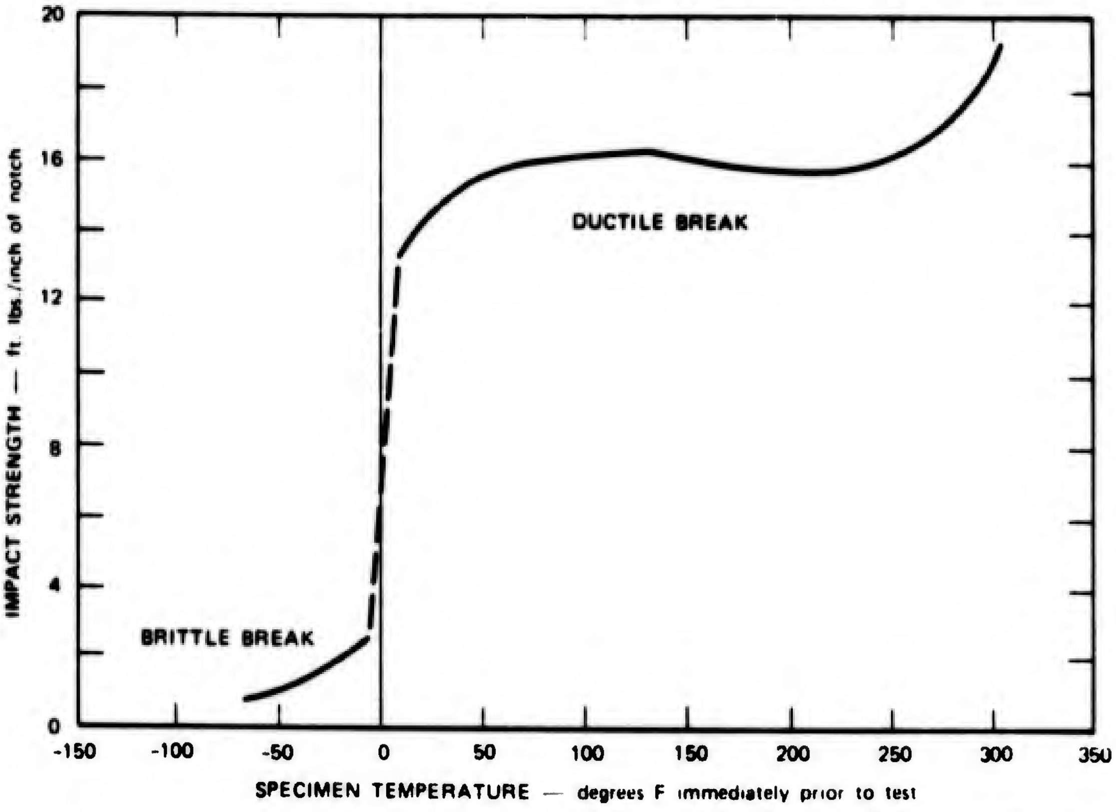

MA-1033-16

FIGURE 1 TTT CURVES FOR POLYCARBONATE

Since polycarbonate exhibits a ductile-brittle transition both with specimen size and with temperature, it is to be expected that a ductile-brittle transition with respect to strain rate will also occur, and predominantly brittle behavior would be observed in the present work at the high strain rates imposed in the gas gun.

For the brittle polymer, P13N polyimide was chosen. In contrast to polycarbonate, polyimide behaves in a brittle fashion even in thin sections and under low strain rates. Its mechanical properties are compared with those of polycarbonate and polymethylmethacrylate (PMMA) in Table I. Polyimide is compatible with all of the commonly used reinforcing fibers and has good thermal stability--prerequisites for its main application as composite matrix material for glass, boron, and carbon fibers at temperatures up to 300°C. The material was supplied by Geigy Industrial Chemicals in the form of molded disks in two thicknesses.

Table I

MECHANICAL AND PHYSICAL PROPERTIES OF THREE POLYMERS

	Ultimate Tensile Strength (Ksi)	Yield Strength (Ksi)	Tensile Elongation (percent)	Young's Modulus (Ksi)	Modulus of Rigidity	Poisson's Ratio	Specific Gravity
Polycarbonate[*]	8.5 - 9.5	8-9	60-100	340	116	0.38	1.2
Polyimide[ø]	11	-	2.50	550	-	0.23[†]	1.33
PMMA[‡]	7 - 10	6-9	2-10	380-450	370-460	-	1.17-1.2

---

[*] LEXAN POLYCARBONATE RESINS, Plastics Department, General Electric, Pittsfield, Mass.

[ø] P13N POLYIMIDE LAMINATING VARNISH, Trade Literature, Geigy Industrial Chemicals, Ardsley, New York.

[†] Calculated from measured sound speeds (see page 6).

[‡] Modern Plastics Encyclopedia, Vol. 47 No. 10A, October 1970.

The velocities of longitudinal and transverse elastic waves in polycarbonate and polyimide were measured in perpendicular directions by the time-in-flight techniques. The results are shown in Table II.

Table II

MEASURED SOUND SPEEDS OF POLYCARBONATE AND POLYIMIDE IN TWO SPECIMEN DIRECTIONS

	Polycarbonate		Polyimide	
	Axial	Radial	Axial	Radial
Longitudinal (mm/μsec)	2.35	2.27	2.52	2.59
Shear (mm/μsec)	1.69	1.76	1.60	1.75

Thus the wave velocities were only slightly anisotropic in these polymers. Thinner disks of polyimide were rather more anisotropic, however.

Experimental Procedure

Short cylindrical specimens 1.5 in. in diameter and 0.25-in. in height were machined from injection-molded polycarbonate sheet stock and from pressed disk-shaped slugs of polyimide, and mounted in a circular holding arrangement at the end of the barrel of the gas gun. The specimens were slightly tapered (8^o) at the edges to allow them to pop out easily under impact and fly into the rags in the catcher tank. The arrangement is shown in Figure 2.

Flat-plate impact was achieved by accelerating a flyer plate against a specimen of the same material. The 2.5-in. diameter by 0.125-in. thick flyer plate was mounted on the end of a 6-in.-long aluminum projectile in which the projectile material immediately behind the flyer plate was removed. Thus the rear surface of the flyer plate was a free surface. To achieve approximately simultaneous contact at all points on the specimen surface by the flyer plate upon impact, the impacting surfaces were ground flat and parallel to at least 0.0005 in.

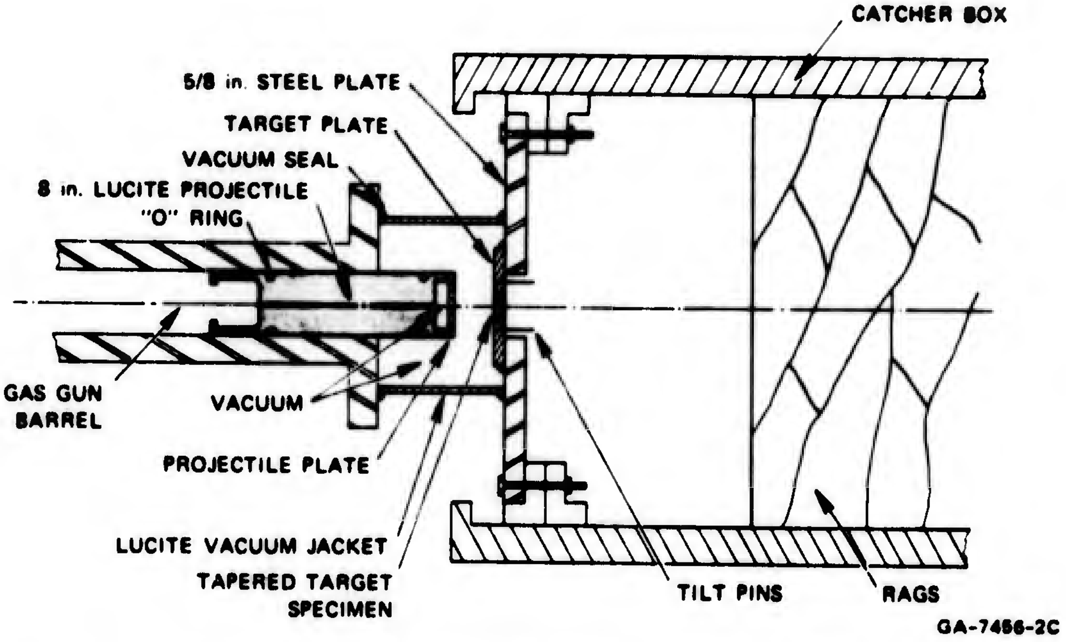

FIGURE 2 EXPERIMENTAL SYSTEM FOR DYNAMIC FLYER PLATE EXPERIMENTS

Compressed helium gas was used to drive the projectile down the 2-1/2-in.-diameter bore of the light gas gun. The gun barrel and the cavity behind the flyer plate were evacuated to a pressure of about 50 to 75μ to eliminate the decelerating effect of a layer of air between flyer plate and specimen prior to impact.

The 8°-taper of the specimen edges facilitated specimen ejection from the holder, and the recovery tank was filled with rags to provide a soft landing and thereby reduce subsequent, unmonitored loading of the specimen. The projectile was prevented from entering the recovery tank by the steel plates shown in the figure. In all cases the specimen and the flyer were recovered after the experiment for examination.

The initial compressive pulse was calculated from the projectile velocity at impact and was used to estimate the tensile stress. Stress relief due to the developing damage was initially neglected. The constitutive relation of each material was obtained in highly instrumented shots, as described later, and the effect of developing damage on the stress histories was estimated in later calculations.

The recovered specimens were sectioned on a diameter, and the section surface was ground and polished to reveal the pattern of cracks. The flyer plates, which experience only compression and hence undergo no tensile damage, were also metallographically examined to determine whether the initial compressive pulse in the specimen alters the material in any observable way.

Estimation of the Impact Velocity Required to Cause Incipient Damage

Before carrying out any experiments with the light gas gun, it is helpful to calculate an approximate value for the projectile velocity sufficient to produce low level shock damage. In the case of polycarbonate, the impact velocity was estimated from stress-particle velocity curves experimentally obtained for PMMA by Barker and Hollenbach,[3] since polycarbonate and PMMA were expected to behave similarly. For the polyimide, no such data were available for comparison and so the impact velocity was estimated in the following way.

The slope of the stress-volume curve is simply related to the density ρ_o and the longitudinal sound speed C_ℓ in the elastic case.

$$\frac{d\sigma}{d(V/V_o)} = -\rho_o C_\ell^2 \tag{1}$$

where V and V_o are the instantaneous and initial specific volumes, respectively. Using the values in Table II we find that

$$\frac{d\sigma}{d(V/V_o)} = -(1.33\ g/cm^3)(2.5 \times 10^5\ cm/sec)^2 = -83\ kbar \tag{2}$$

Then, assuming that under dynamic loading conditions polyimide behaves elastically, we can write

$$\sigma = (83\ kbar)(1-V/V_o) \tag{3}$$

Now substituting this relation into the expression for the particle velocity u

$$u = [\frac{\sigma}{\rho_o}(1-V/V_o)]^{1/2} \tag{4}$$

we obtain

$$u = \sigma(\rho_o \times 83 \text{ kbar})^{-1/2}$$

or

$$\sigma = (3.3 \times 10^{-4})u \tag{5}$$

where σ has units of kbar and u is in cm/sec. The static tensile strength of polyimide is 11,000 psi or 0.76 kbar (Table I), and the Poisson ratio ν may be calculated from the measured sound speeds

$$\nu = \frac{\frac{1}{2}(C_\ell/C_s)^2-1}{(C_\ell/C_s)^2-1} \tag{6}$$

to be about

$$\nu = \frac{0.5(2.7/1.6)^2-1}{(2.7/1.6)^2-1} = 0.23 \tag{7}$$

So the Hugoniot elastic limit is

$$\text{HEL} = \frac{1-\nu}{1-2\nu} \approx 1.43 \text{ Y or about 1 kbar}$$

where the static yield strength Y has been approximated by the tensile strength. This requires a particle velocity of about 33 m/sec according to Eq. (5) or an impact velocity of 60 m/sec, since the particle velocity is about half the impact velocity.

Tapered Flyer Shots

An expedient experimental method which yields a good estimate of the threshold stress entails impacting the specimen with a tapered flyer plate. By this impact configuration, sketched in Figure 3, the time at stress varies across the diameter of the specimen as depicted in Figure 4.

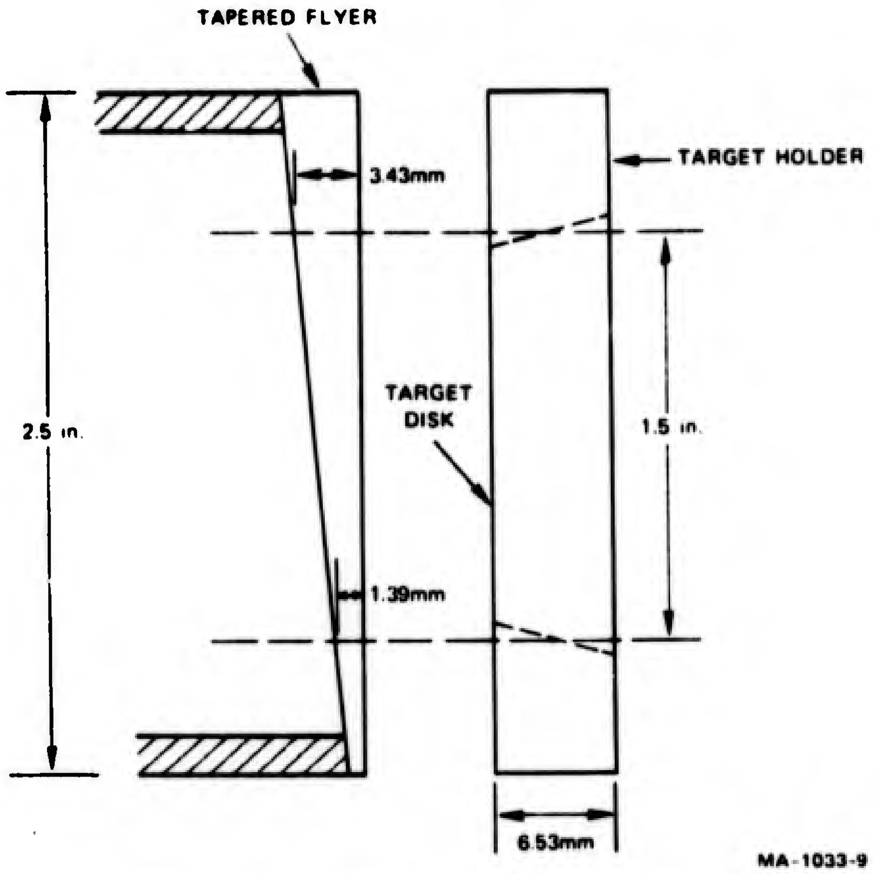

FIGURE 3 TAPERED FLYER IMPACT EXPERIMENT

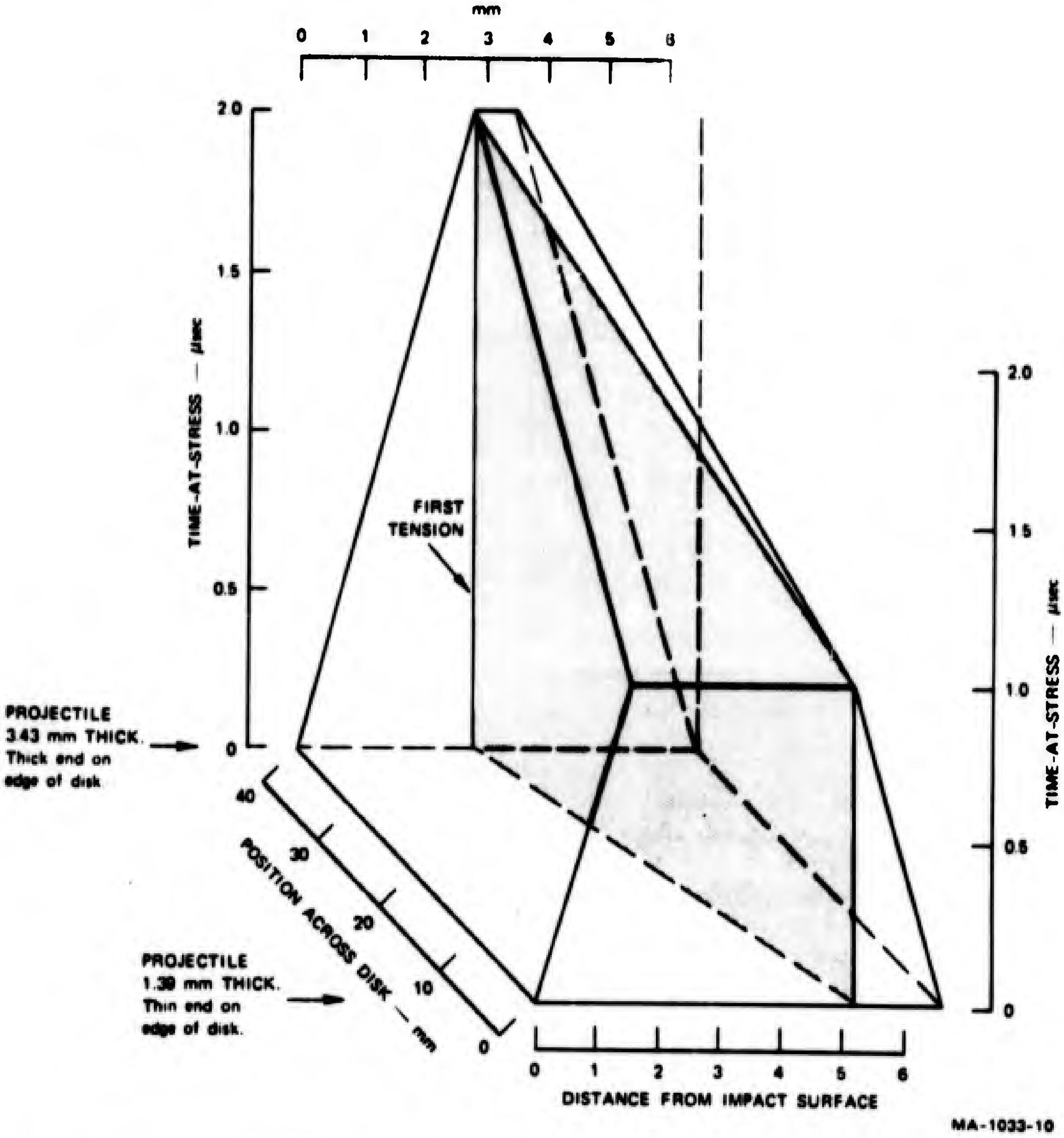

FIGURE 4 STRESS DURATION IN SPECIMEN IMPACTED WITH A TAPERED FLYER

Hence the level of damage also varies across the specimen and the stress-stress duration point corresponding to threshold damage can be determined. This method allows a rapid survey of a new material, and identifies the experimental conditions necessary for the flat flyer shots to provide more detailed data.

Impact Experiments

Thirteen impact experiments were carried out in the 2-1/2-in. bore diameter light gas gun during the course of this work. These experiments included one gaged shot on each material to determine the stress-volume relations during dynamic loading and unloading, four tapered flyer shots on polycarbonate to expedite determination of the threshold stress, and seven uninstrumented recovery shots for quantitative damage analyses. A summary of the shots is given in Table III.

When possible, the fracture damage produced by the stress waves was quantitatively assessed in the following manner. Impacted and recovered specimen disks were sectioned on a diameter and the section surface was ground and polished to reveal the crack pattern. Composite micrographs of this surface were made at nominal magnifications of about 200X, the number of cracks intersecting the surface of polish was recorded, and their lengths, widths, and orientations were measured as a function of position in the sample. The BABS2 computer code[2] was used to transform the surface distributions into volume distributions, and NAG functions for fracture damage were then extracted from correlations of these distributions and the computed stress histories.

Table III

SUMMARY OF FLAT-PLATE IMPACT EXPERIMENTS

Shot No.	Material (of flyer and target)	Flyer Thickness (mm)	Target Thickness (mm)	Impact Velocity (m/sec)	Comments
1	Polycarbonate	0.763 - 4.06	6.35	68.7	Tapered flyer shot.
2	Polycarbonate	0.763 - 4.06	6.35	155	Tapered flyer shot.
3	Polycarbonate	0.763 - 4.06	6.35	117	Tapered flyer shot.
4	Polycarbonate	0.763 - 4.06	6.35	145	Tapered flyer shot.
5	Polycarbonate	3.18	6.35	152	Recovery shot for quantitative analysis.
6	Polycarbonate	3.18	6.35	142	Recovery shot for quantitative analysis.
7	Polycarbonate	3.18	6.35	137	Recovery shot for quantitative analysis.
8	Polyimide	2.49	5.70	92.7	Recovery shot for quantitative analysis.
9	Polyimide	2.49	5.70	69.5	Recovery shot for quantitative analysis.
10	Polyimide	2.49	5.70	63.0	Recovery shot for quantitative analysis.
11	Polyimide	2.49	5.70	68.0	Recovery shot for quantitative analysis.
12	Polycarbonate	3.18	(See Fig.5)	361	Particle velocity gages to measure loading and unloading paths.
13	Polyimide	3.18	(See Fig.8)	276	Stress gages to measure loading and unloading paths.

Measurement of Constitutive Relations

The NAG method for predicting shock damage requires that the stress histories in impacted samples be known. We therefore need to know the constitutive relations for polycarbonate and polyimide. The scope of the present project did not allow a sufficient experimental program to determine precise constitutive relations; however, we obtained estimates by combining static uniaxial strain compression measurements with one instrumented dynamic experiment for each material. In the static experiments the samples were subjected to uniaxial strain compression and release cycles in a large press. The experimental arrangement is documented elsewhere.[2] Samples of polycarbonate and polyimide were loaded statically and isothermally to compressive stress levels of about 5 kbar, and then released. Control samples of PMMA were also tested in this way, since a large amount of static and dynamic data is available for this material.

One instrumented impact experiment was performed on specimens of each material to determine the dynamic loading and unloading paths at compressive stresses to about 5 kbar. The instrumented polycarbonate experiment is illustrated in Figure 5. Three electromagnetic in-material particle velocity gages were used, and a laser interferometer monitored the particle velocity in the plane of the third electromagnetic gage. The first electromagnetic gage failed to record, but good records were obtained from gages 2 and 3. The laser interferometer[3] record had a high noise level,but was consistent with the record from the third electromagnetic gage. The oscilloscope records from gages 2 and 3 are shown in Figure 6, and the laser interferometer record together with a comparison with the results from the velocity gage record are shown in Figure 7. A Lagrangian analysis[4,5] was used on these records to obtain the loading and unloading curves in both stress-particle velocity and stress-volume space.

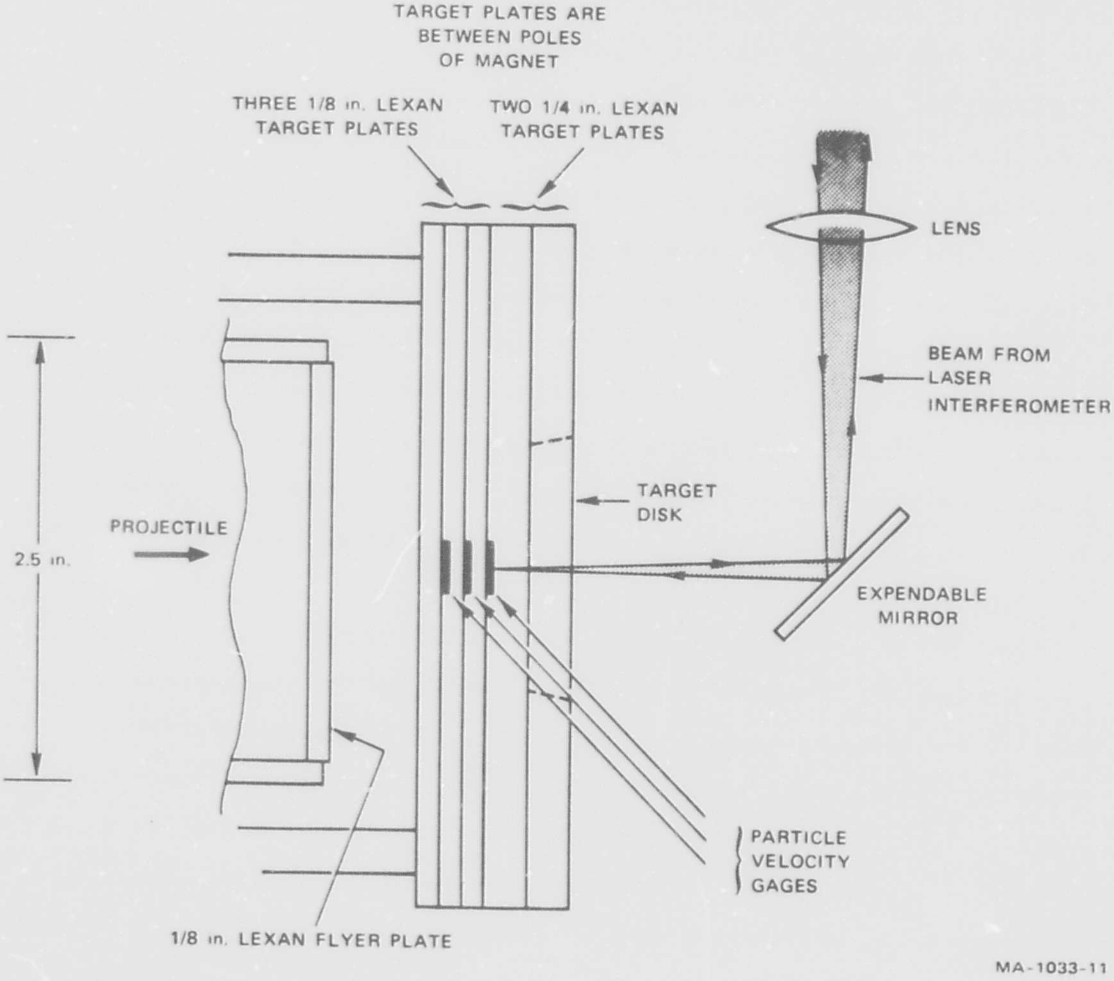

FIGURE 5 ARRANGEMENT FOR INSTRUMENTED IMPACT EXPERIMENT ON POLYCARBONATE

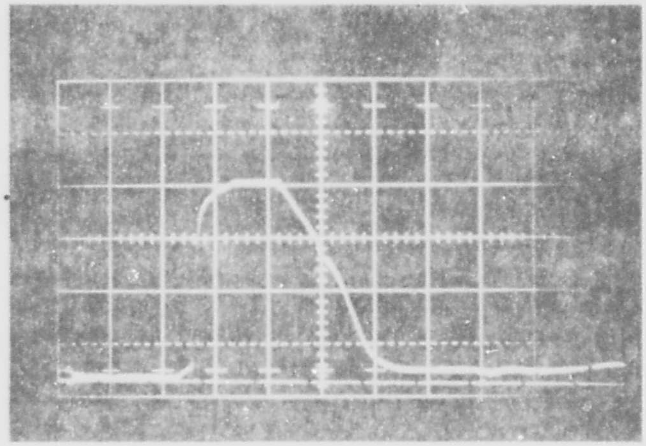

(a) GAGE 2, 1 μsec/division

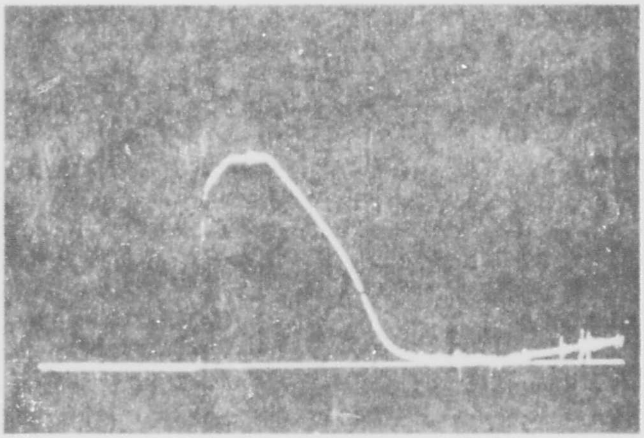

(b) GAGE 3, 1 μsec/division

MP-1033-12

FIGURE 6 OSCILLOSCOPE RECORDS FROM ELECTROMAGNETIC PARTICLE VELOCITY GAGES No. 2 AND 3 IN POLYCARBONATE SAMPLE

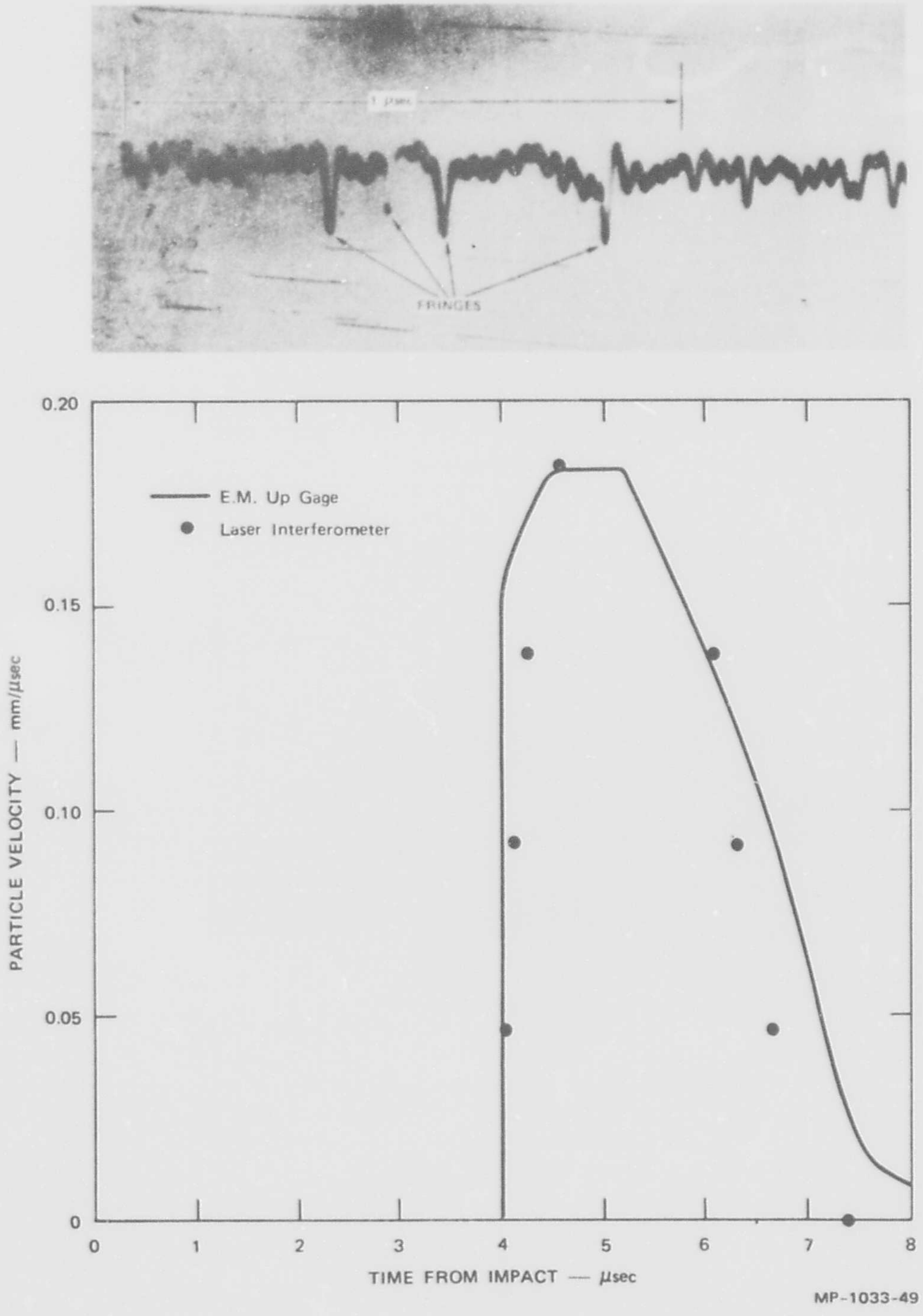

FIGURE 7 COMPARISON OF PARTICLE VELOCITY HISTORIES FROM LASER INTERFEROMETER AND ELECTROMAGNETIC GAGES

The instrumented experiment performed on polyimide for which ytterbium stress gages were used is illustrated in Figure 8 and the oscilloscope records are shown in Figure 9. The second stress gage record in Figure 9 shows unexpected structure on both the loading and release segments. This anomalous behavior of the second gage precluded application of Lagrangian methods to obtain the stress-volume loading and unloading paths in the material. However, the successful recording of the first gage makes it possible to check the consistency of an assumed constitutive relation, as is done in the next section.

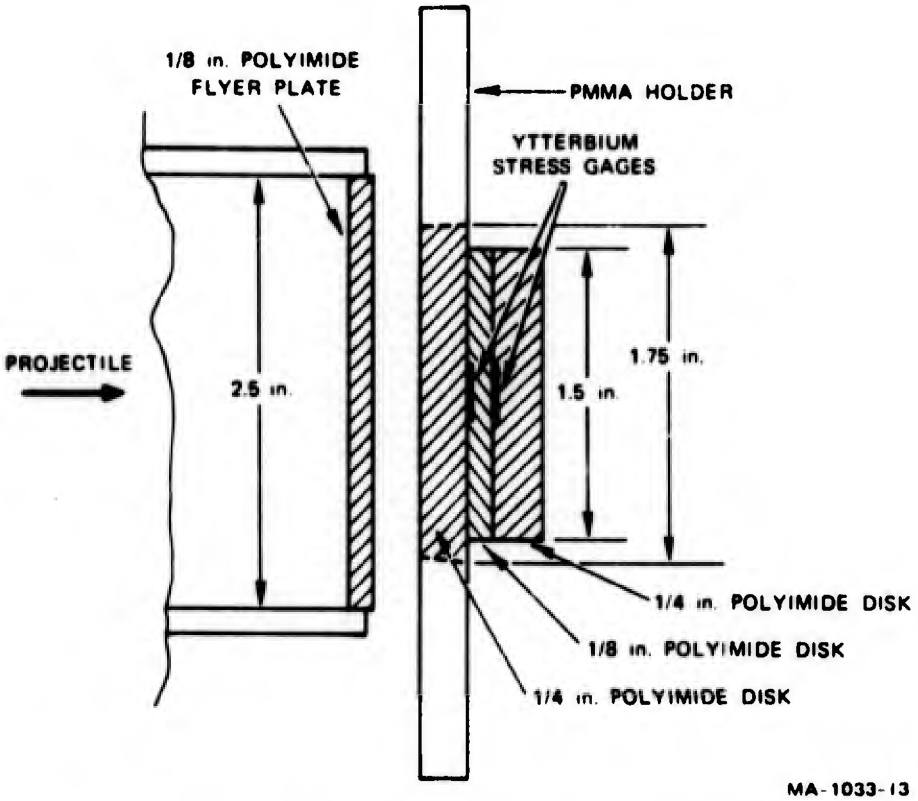

FIGURE 8 ARRANGEMENT FOR INSTRUMENTED IMPACT EXPERIMENT ON POLYIMIDE

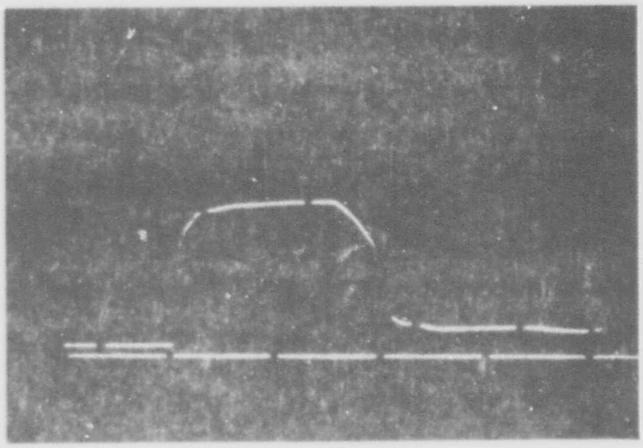

(a) GAGE 1, 1 μsec/division

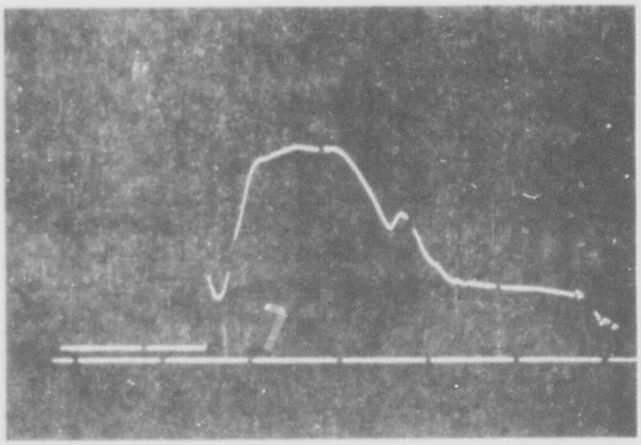

(b) GAGE 2, 1 μsec/division

MP-1033-14

FIGURE 9 OSCILLOSCOPE RECORDS FROM Yb STRESS GAGES IN POLYIMIDE SAMPLE

III RESULTS

Constitutive Relation for Polycarbonate

The results of the dynamic and static experiments on polycarbonate are summarized in Figure 10. The constitutive relation was constructed from these data in the following way. First, the Hugoniot curve was assumed to be identical with the static loading curve. It is seen that the peak compressive stress reached in the dynamic experiment lies on a reasonable extrapolation of the static curve. The Hugoniot curve thus obtained can be described by the equation

$$\sigma_H = (4.72)(10^{10})\mu - (1.33)(10^{11})\mu^2 + (3.5)(10^{12})\mu^3 \ \frac{\text{dynes}}{\text{cm}^2} \qquad (8)$$

where $\mu = \frac{\rho}{\rho_o} - 1$. Next, the observed dynamic unloading curve was assumed to be an isentrope. We further assume that the material has a negligible yield stress, so that the equilibrium stress tensor is almost hydrostatic and that the material can be described by a Mie-Grüneisen equation of state,

$$\sigma - \sigma_H = (\frac{\Gamma}{V})\ (E-E_H) \qquad (9)$$

where E is the internal energy and Γ is the Grüneisen coefficient. The difference in the areas under the Rayleigh line and the dynamic unloading curves was used to evaluate $E - E_H$ in the above equation, and the difference $\sigma - \sigma_H$ at $V/V_o = 1$ could be measured. In this way the value of Grüneisen's ratio Γ was found to be 1.3, in good agreement with values reported for other polymers.[6]

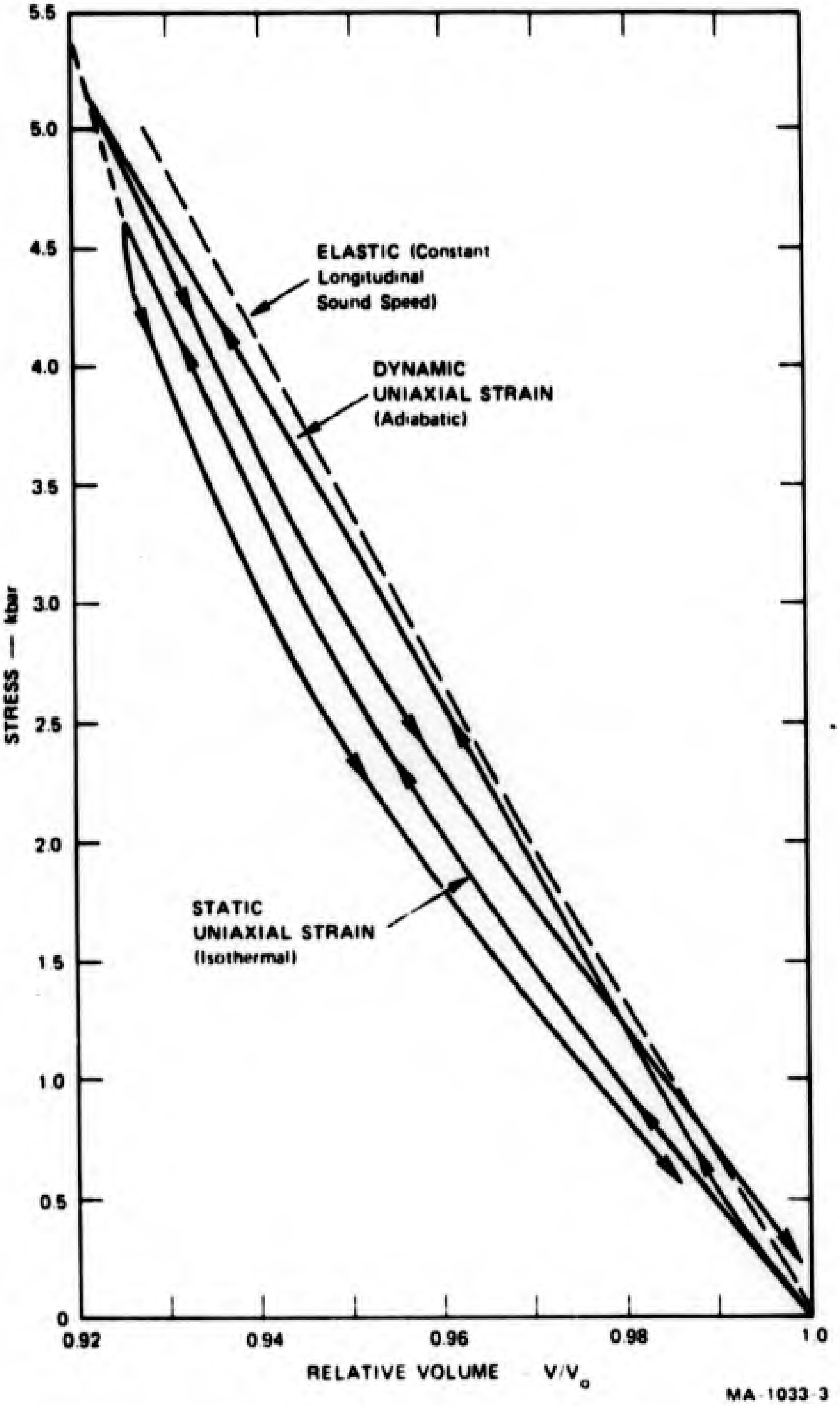

FIGURE 10 STATIC AND DYNAMIC UNIAXIAL STRAIN LOADING AND UNLOADING CURVES FOR POLYCARBONATE

Polymers often behave in a viscoelastic manner at stresses of a few kilobars.[3,7-9] The particle velocity and stress records of Figures 6 and 9 are in fact typical of viscoelastic materials, consisting of a sharp rise followed by a slower approach to the maximum amplitude. Comparison of the records of Figure 6 reveals that the shape of the shock front has not changed between gages, thus indicating that a steady state has already been reached after the shock has traveled 3 mm. The constitutive relation used to describe polycarbonate was the hydrodynamic equation of state given by Eqs. (8) and (9) plus a viscous stress given by the artificial viscosity normally used in the PUFF code. The viscoelastic behavior was not treated explicitly because of a lack of information on the rate-dependent mechanism of polycarbonate.

Constitutive Relation for Polyimide

The results of the dynamic and static experiments on polyimide are summarized in Figure 11. The anomalous record from the second stress gage in the gaged polyimide shot made it impossible to get the loading and unloading curves in the stress-volume plane. However, in view of the polycarbonate results, we assumed that the measured static loading curve is identical with the Hugoniot curve, and that a steady shock wave was attained before the shock reached the first gage. Thus, we assume that the dynamic loading curve to the peak stress of 4.2 kbar recorded by the first gage is given by the Rayleigh line, as shown in Figure 11. The static loading curve, now assumed to be the Hugoniot, is well represented by the equation

$$\sigma = (6.30)(10^{10})\mu + (1.09)(10^{11})\mu^2 + (3.40)(10^{12})\mu^3 \text{ dynes/cm}^2 \quad (10)$$

For lack of better information, the unloading isentrope was assumed to be coincident with the assumed Hugoniot curve. This assumption holds reasonably well for relatively incompressible materials. Comparison of Figures 10 and 11 shows that the polyimide is appreciably stiffer than the polycarbonate, thus suggesting that the above approximation is more accurate for polyimide than it would have been for polycarbonate.

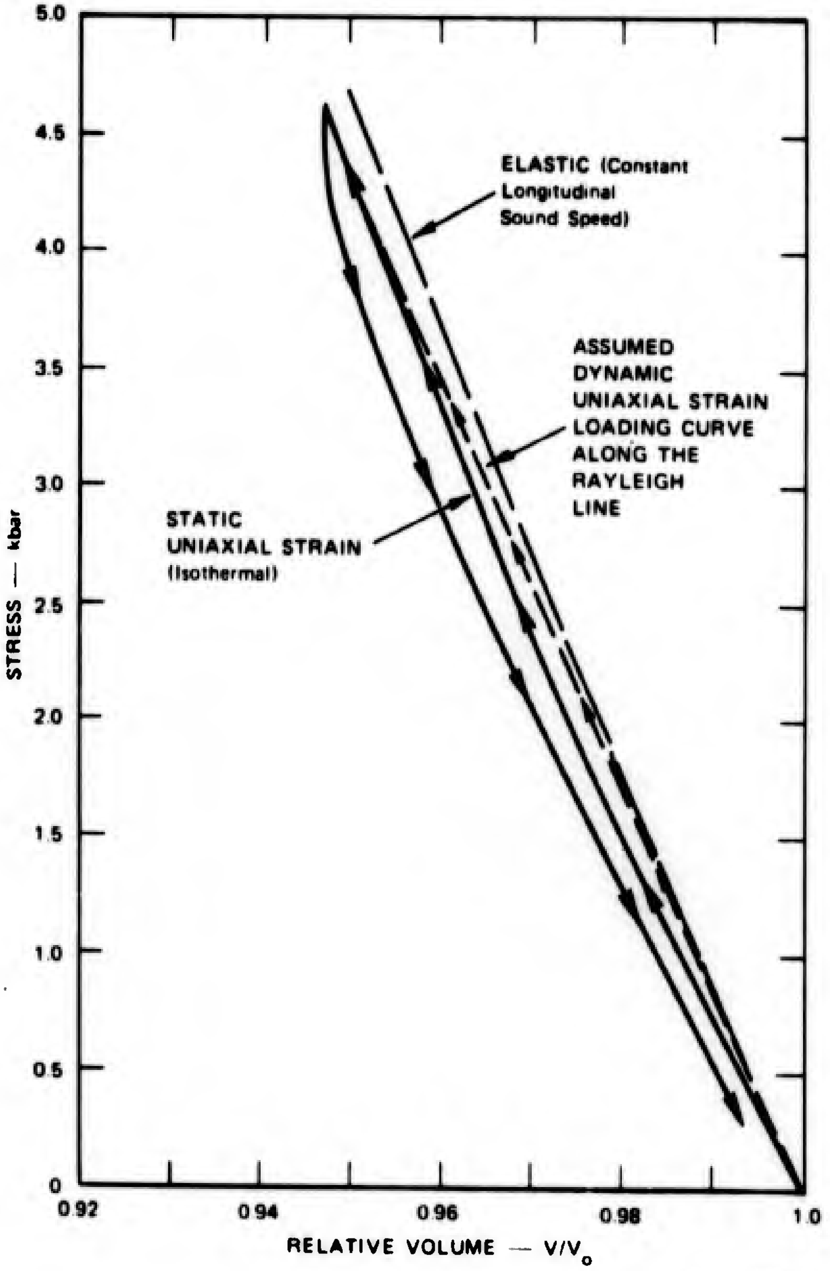

MA-1033-15

FIGURE 11 STATIC AND DYNAMIC UNIAXIAL STRAIN LOADING AND UNLOADING CURVES FOR POLYIMIDE

Thus, insufficient dynamic data have made it necessary to postulate for polyimide a constitutive relation which is based mainly on plausibility arguments. As was the case for polycarbonate, the material is assumed to have negligible strength, and to follow a Mie-Grüneisen equation of state. In view of the uncertainties in the above constitutive relation for polyimide, it is advisable to check the relation by testing its ability to predict the stress-time record from the first gage. This has been done, and the results are shown in Figure 12.

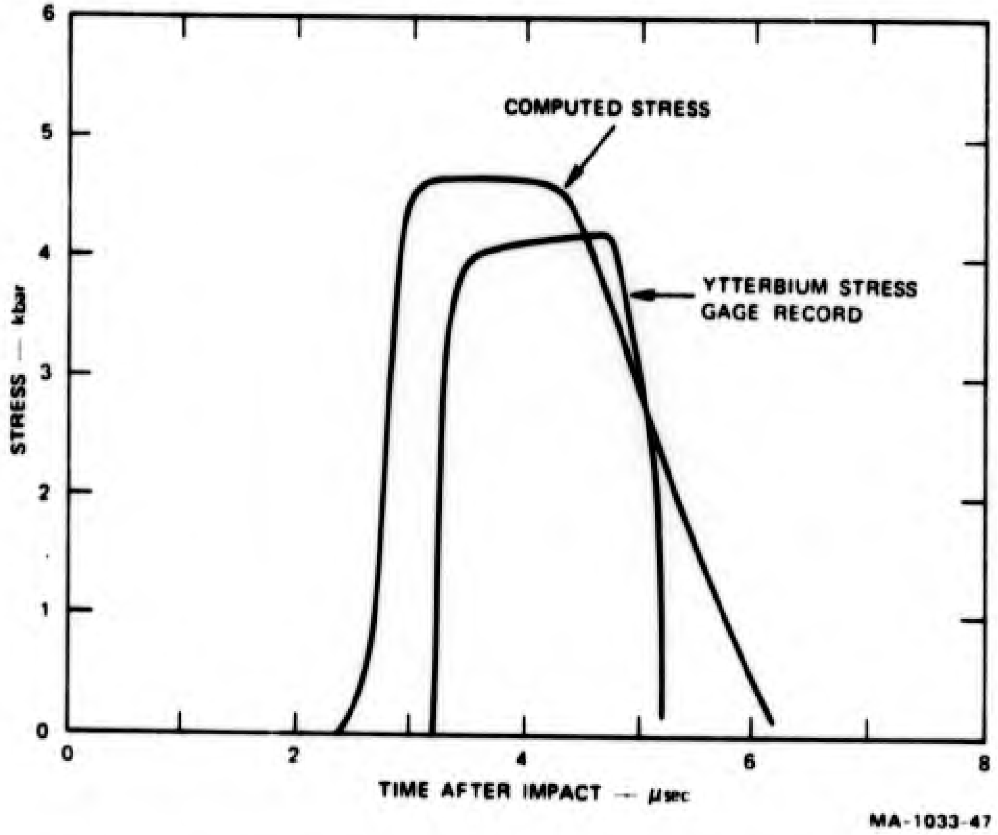

FIGURE 12 COMPARISON OF COMPUTED AND MEASURED STRESS HISTORY IN POLYIMIDE

As can be seen, the agreement is fair, but significant differences in both amplitude and arrival time exist. The computed stress history is typical for a material which loads along the Rayleigh line and unloads along an isentrope which is concave upward . The initial unloading velocity is much higher than that at low stress, and hence, the unloading wave is a long ramp. The stress gage record, on the other hand, shows an unloading path which is comparable in duration to the loading path; hence the actual unloading path must be nearly straight. The computed stress arrives earlier and attains a higher amplitude, suggesting that the computational model is too stiff. Several more experiments with multiple in-material stress or particle velocity gages would be required to obtain a better constitutive relation for this material.

Comparison of Polycarbonate and Polyimide Constitutive Relations With Those for PMMA

It is of interest to compare the foregoing results for polycarbonate and polyimide with those of previous workers for PMMA. In Figure 13 we compare our measured static loading and unloading curves with a dynamic loading and unloading curve from Barker and Hollenbach.[3] PMMA is apparently much more rate dependent than polycarbonate or polyimide, and its dynamic curves lie to the right of the zero pressure elastic curve, indicating that the PMMA Hugoniot is strongly concave upward. In fact, the dynamic unloading curve in Figure 13 follows very closely the Hugoniot curve measured by Barker and Hollenbach for PMMA in this stress region. The large difference between the Hugoniot curve (reached by adiabatic paths) and the static isothermal curve was unexpected. The validity of our static measurements is supported by the agreement with Bridgman's data (one Bridgman point is shown in Figure 13), and we therefore believe that this large difference is real.

It appears then that a basic difference exists in the dynamic response of PMMA and that of polycarbonate or polyimide. It would be of interest to investigate this question in more detail.

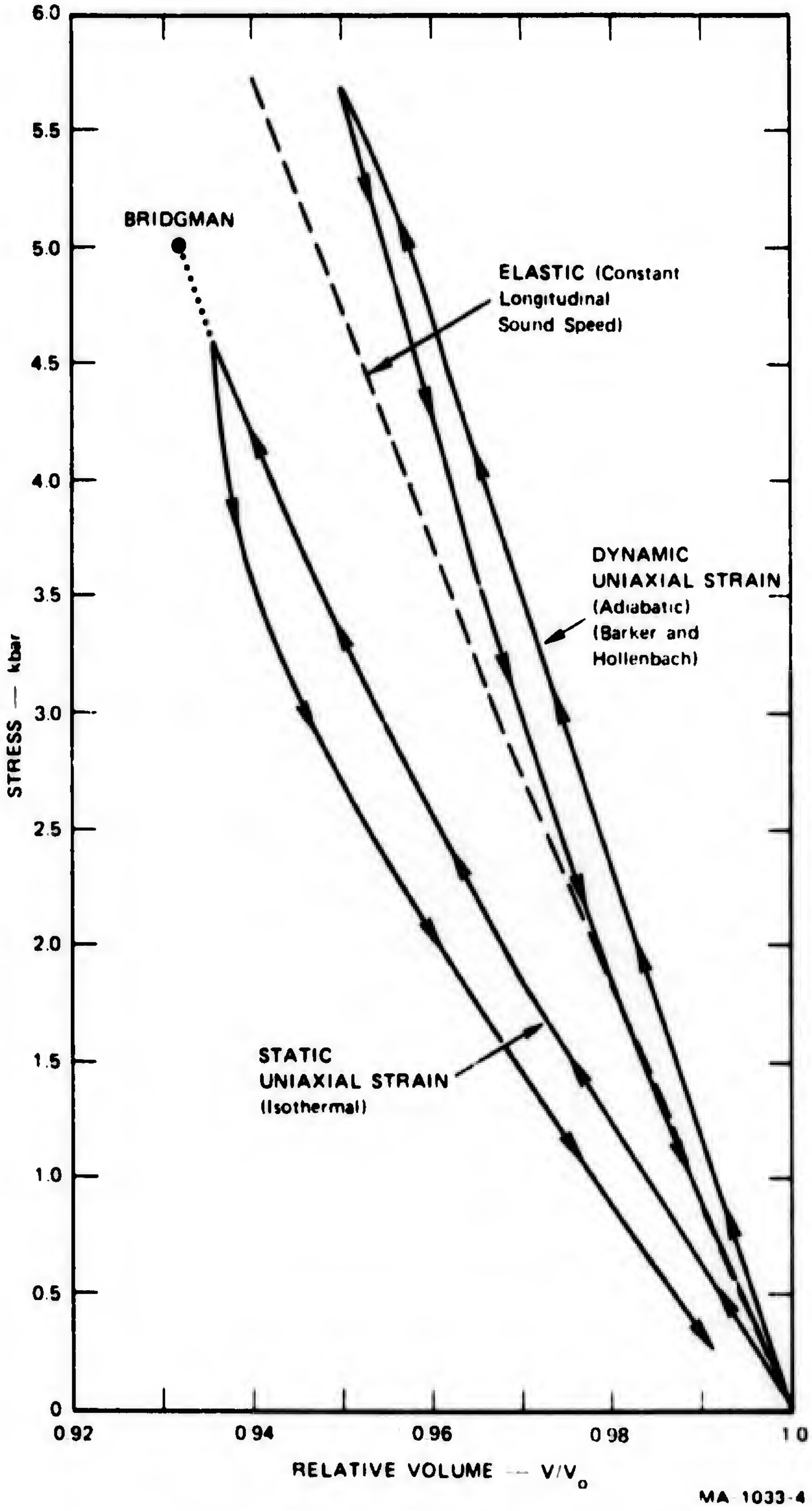

FIGURE 13 STATIC AND DYNAMIC UNIAXIAL STRAIN LOADING AND UNLOADING CURVES FOR PMMA

Damage Distributions from Impact Experiments

Micrographs of the fracture damage revealed by sectioning specimens 5 and 6 are shown in Figures 14 and 15. The raw data consisted of the number, length, and distance from the plane of maximum stress duration of these crack traces (Tables IV and V). The number of crack traces versus zone position for polycarbonate specimens impacted at velocities of 152 and 142 m/sec (peak stresses of 1.76 and 1.66 kbar) is plotted in Figures 16 and 17. These figures show that the number of crack traces lying in equisized zones is a maximum near the plane of maximum stress duration and falls off rapidly with distance from this plane. Figures 18 and 19 show the size distribution of crack traces for the same two specimens.

The surface distributions were transformed into volume distributions by means of the BABS2 computer code and the results are presented in Figures 20 and 21, for specimens 5 and 6. For convenience in extracting nucleation and growth rate parameters, the results are presented as cumulative number of cracks having a radius greater than some radius R for various stress durations (zone position).

In the case of specimen 7 (Fig. 27), it was possible with the microscope to distinguish individual cracks and measure their radii and positions with respect to the plane of maximum stress duration without sectioning, thus determining the volume distributions directly. This was such a low damage level shot however, (48 cracks), that a statistical treatment of crack concentration per zone was impossible.

As will be discussed later in Section IV, cracks in polycarbonate typically assumed a dish-shaped profile (Figure 38) and there was some question as to the length to be measured. The length segments AB, BC, and CD were all measured and the data were analyzed both in terms of the total length ABCD and the middle segment BC. No large differences in either the surface or volume distributions resulted. The results presented in this report were derived using the length ABCD as the crack length.

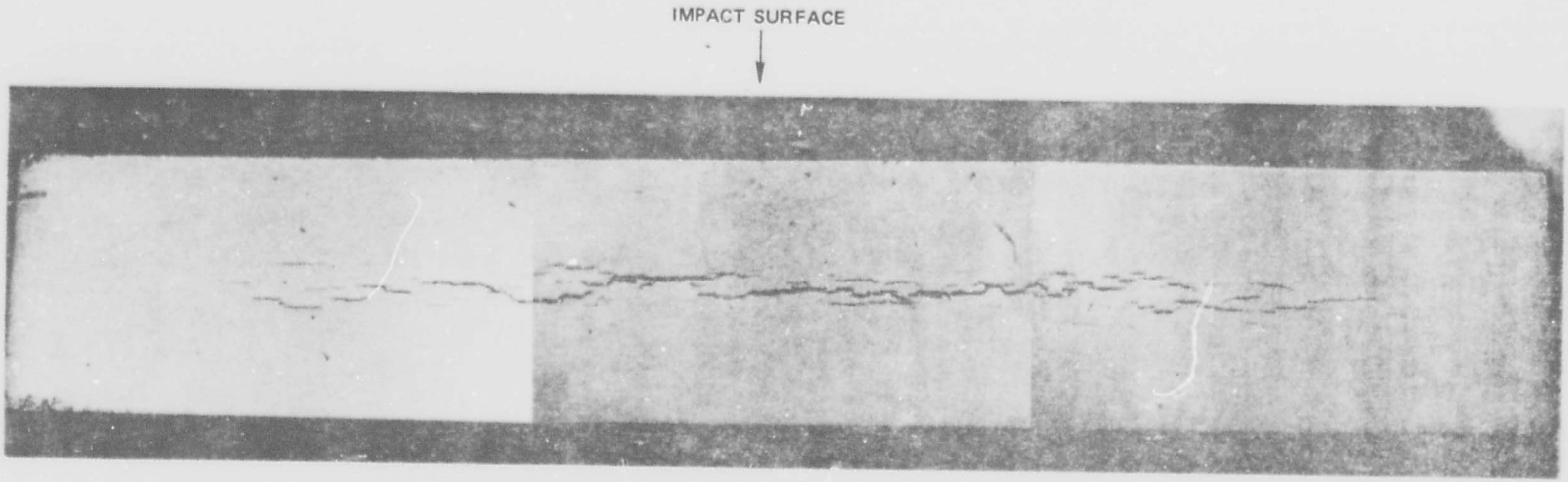

MP-1033-38

FIGURE 14 POLISHED SECTION THROUGH POLYCARBONATE SPECIMEN NO. 5 SHOWING THE DISTRIBUTION OF CRACK TRACES INTERSECTING THE SURFACE

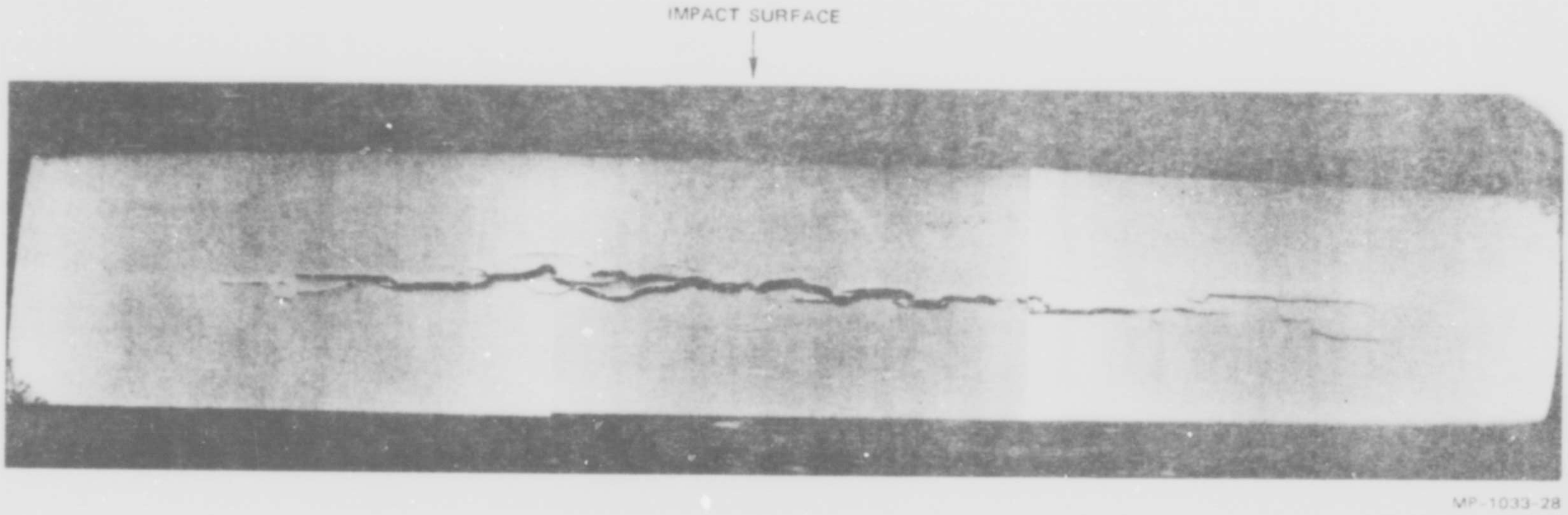

FIGURE 15 POLISHED SECTION THROUGH POLYCARBONATE SPECIMEN NO. 6 SHOWING THE DISTRIBUTION OF CRACKS INTERSECTING THE SURFACE

Table IV

SIZE DISTRIBUTION OF CRACK TRACES ON SECTIONED SURFACE OF SPECIMEN NO. 5

Zone Number (From Free Surface)	Length Interval in cm at 70X										
	0.0-0.3	0.3-0.6	0.6-1.1	1.1-1.7	1.7-2.5	2.5-3.7	3.7-5.3	5.3-7.4	7.4-10.4	10.4-14.3	Total in Zone
1	0	0	0	0	1	0	0	0	0	0	1
2	0	0	1	1	0	1	0	0	1	0	4
3	0	0	2	0	1	0	0	0	0	0	3
4	0	0	4	3	4	1	1	0	0	0	13
5	0	0	1	1	4	2	1	0	0	0	9
6	0	4	3	6	6	4	7	2	1	0	33
7	1	6	2	7	3	3	0	1	0	0	23
8	0	1	2	2	5	7	1	2	0	0	20
Spall Plane											
9	0	1	0	7	4	7	7	5	0	0	31
10	0	1	3	2	3	6	1	0	0	0	16
11	1	4	5	7	7	4	3	2	0	0	33
12	0	2	4	5	8	5	5	0	0	0	29
13	0	0	2	4	4	3	0	1	0	0	14
14	0	1	0	3	1	3	4	1	0	1	14
15	0	0	1	1	1	2	1	0	0	0	6
16	0	1	0	0	0	0	1	0	0	0	2
17	0	0	0	0	0	0	2	0	0	0	2
18	0	0	0	0	2	0	0	0	0	0	2
19	0	0	0	1	0	0	0	0	0	0	1
Total in Length Interval	2	21	30	50	54	48	34	14	2	1	256

Table V

SIZE DISTRIBUTION OF CRACK TRACES ON SECTIONED SURFACE OF SPECIMEN NO. 6

Zone Number (From Free Surface)	Length Interval in cm at 70X										
	0.0-0.2	0.2-0.5	0.5-0.9	0.9-1.5	1.5-2.4	2.4-3.7	3.7-5.5	5.5-8.2	8.2-12.1	12.1-17.8	Total in Zone
1	0	0	0	0	0	0	0	0	0	0	0
2	0	0	0	0	0	0	0	0	0	1	1
3	0	0	0	0	0	0	0	0	0	0	0
4	0	0	1	0	2	0	0	0	0	0	3
5	0	0	0	1	0	1	0	0	2	0	4
6	0	0	0	2	2	1	2	0	4	0	11
7	0	0	1	2	2	1	3	2	1	0	12
8	1	2	1	1	1	2	1	2	1	1	13
Spall Plane											
9	0	0	0	0	1	0	1	1	2	1	6
10	0	0	0	1	1	1	1	4	0	0	8
11	0	0	0	0	0	0	4	2	0	0	6
12	0	0	0	0	1	0	2	2	0	0	5
13	0	0	0	1	0	0	0	1	0	0	2
14	0	0	0	0	0	0	1	1	0	0	2
15	0	0	0	0	0	0	0	0	0	1	1
16	0	0	0	0	0	0	0	0	0	0	0
Total in Length Interval	1	2	3	8	10	6	15	15	10	4	74

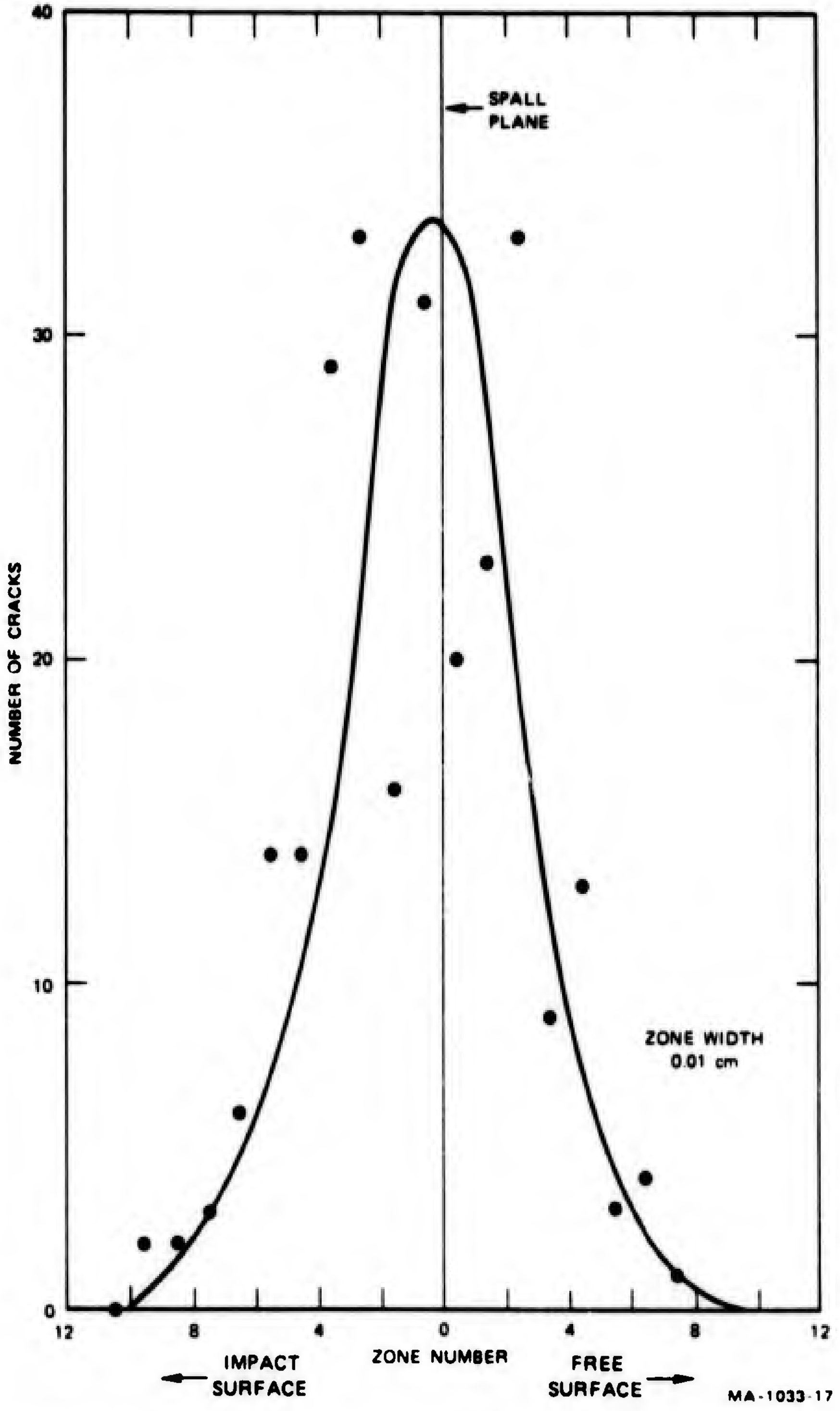

FIGURE 16 VARIATION OF THE NUMBER OF CRACK TRACES ON A DIAMETRICAL SECTION IN IMPACTED POLYCARBONATE SPECIMEN NO. 5 WITH DISTANCE FROM THE PLANE OF MAXIMUM STRESS DURATION

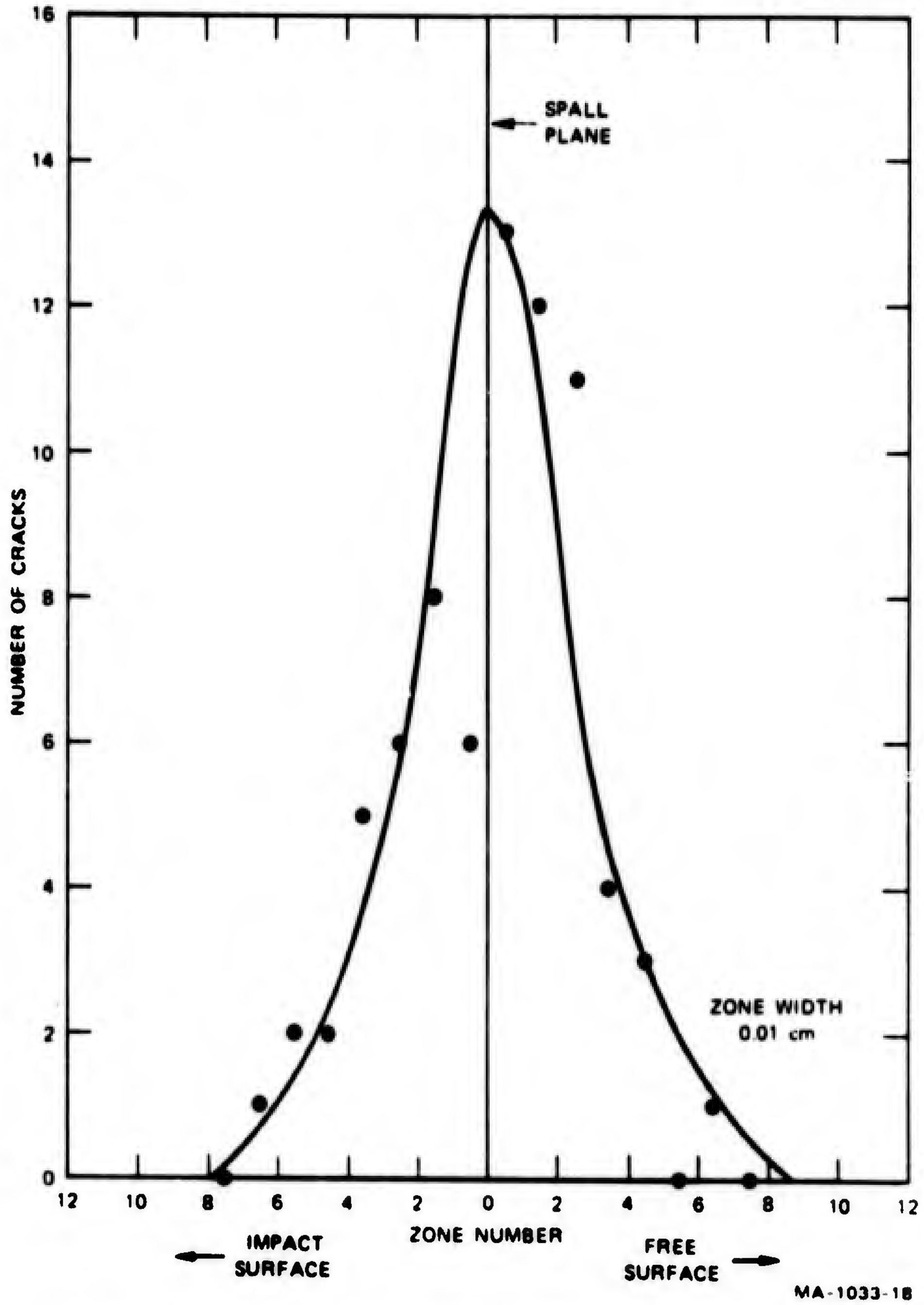

FIGURE 17 VARIATION OF THE NUMBER OF CRACK TRACES ON A DIAMETRICAL SECTION IN IMPACTED POLYCARBONATE SPECIMEN No. 6 WITH DISTANCE FROM THE PLANE OF MAXIMUM STRESS DURATION

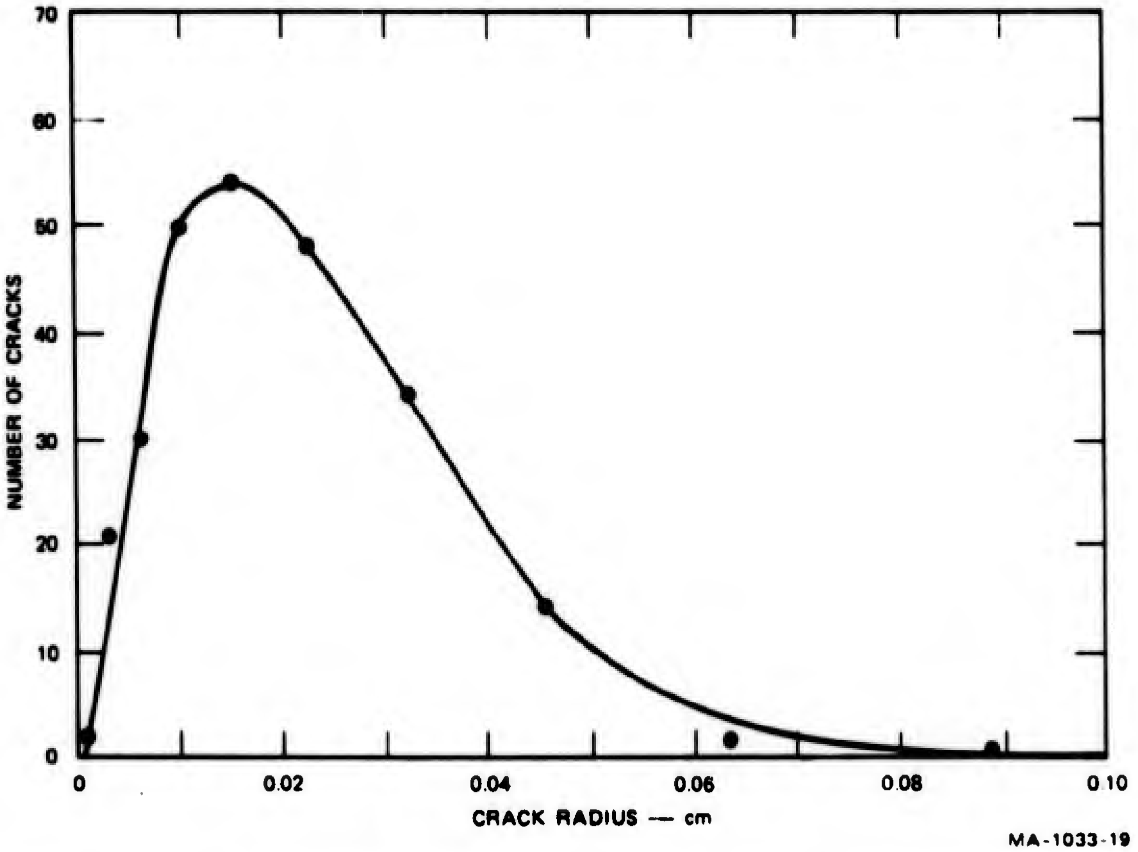

FIGURE 18 THE SIZE DISTRIBUTIONS OF CRACK TRACES MEASURED ON A DIAMETRICAL SECTION IN IMPACTED POLYCARBONATE SPECIMEN No. 5

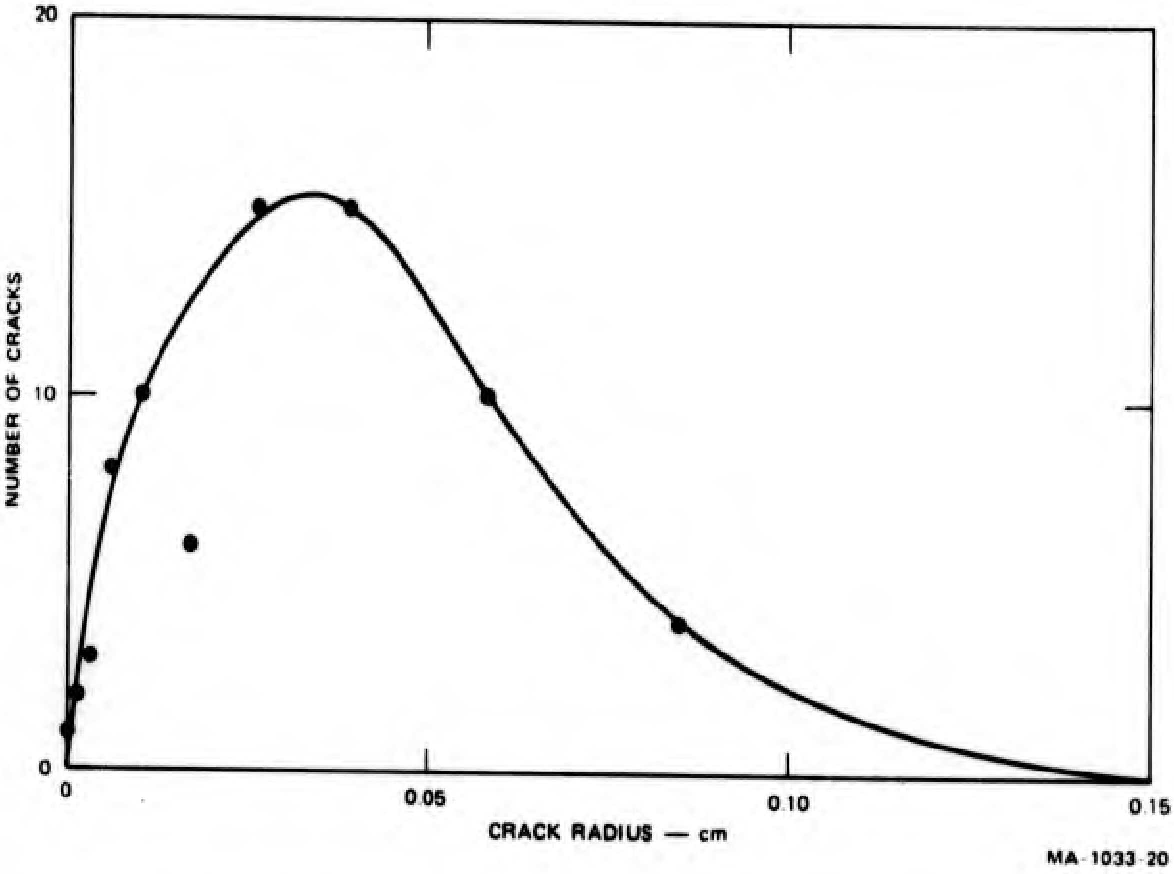

FIGURE 19 THE SIZE DISTRIBUTIONS OF CRACK TRACES MEASURED ON A DIAMETRICAL SECTION IN IMPACTED POLYCARBONATE SPECIMEN No. 6

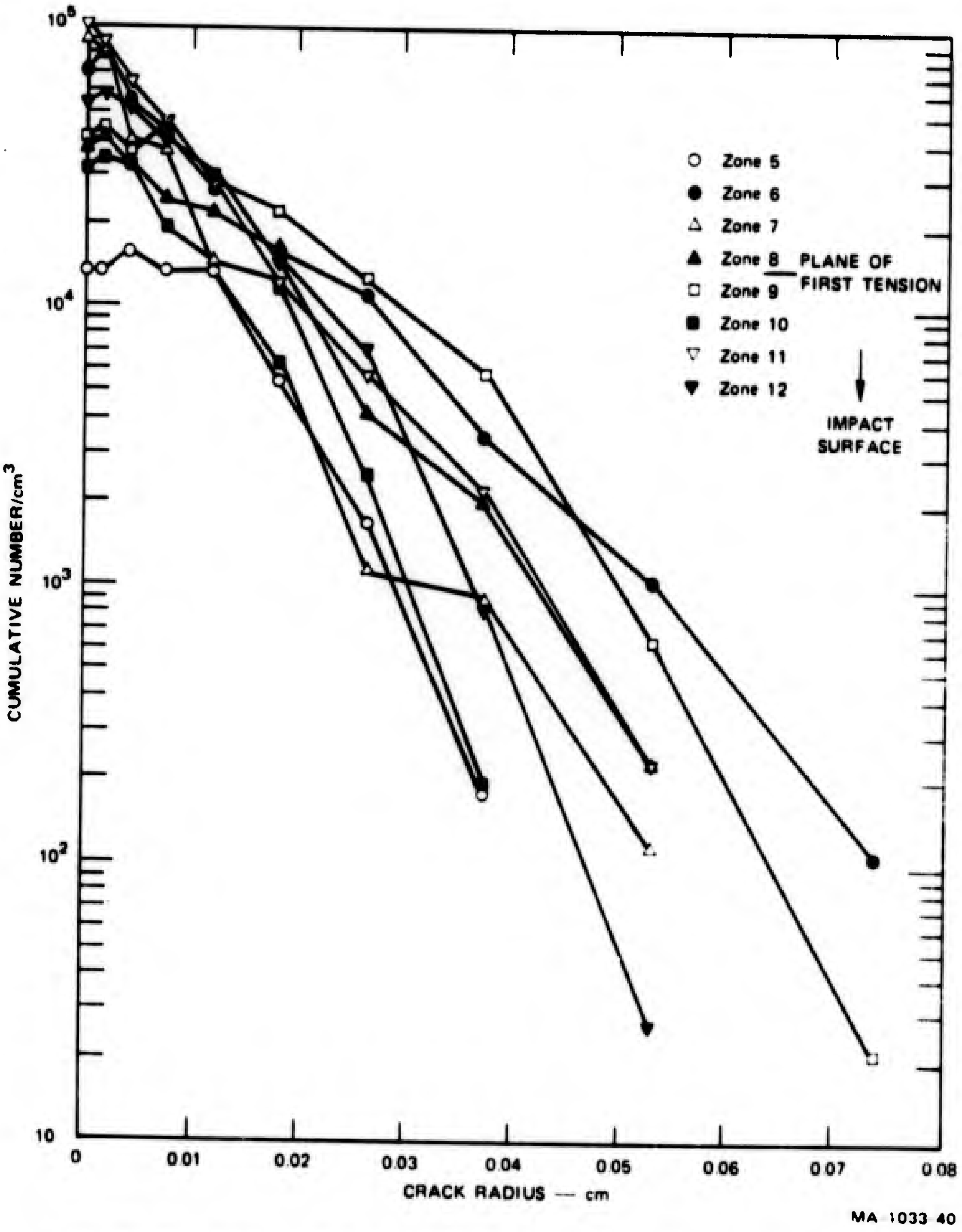

FIGURE 20 SIZE DISTRIBUTION OF CRACKS IN POLYCARBONATE SPECIMEN No. 5 AS A FUNCTION OF STRESS DURATION

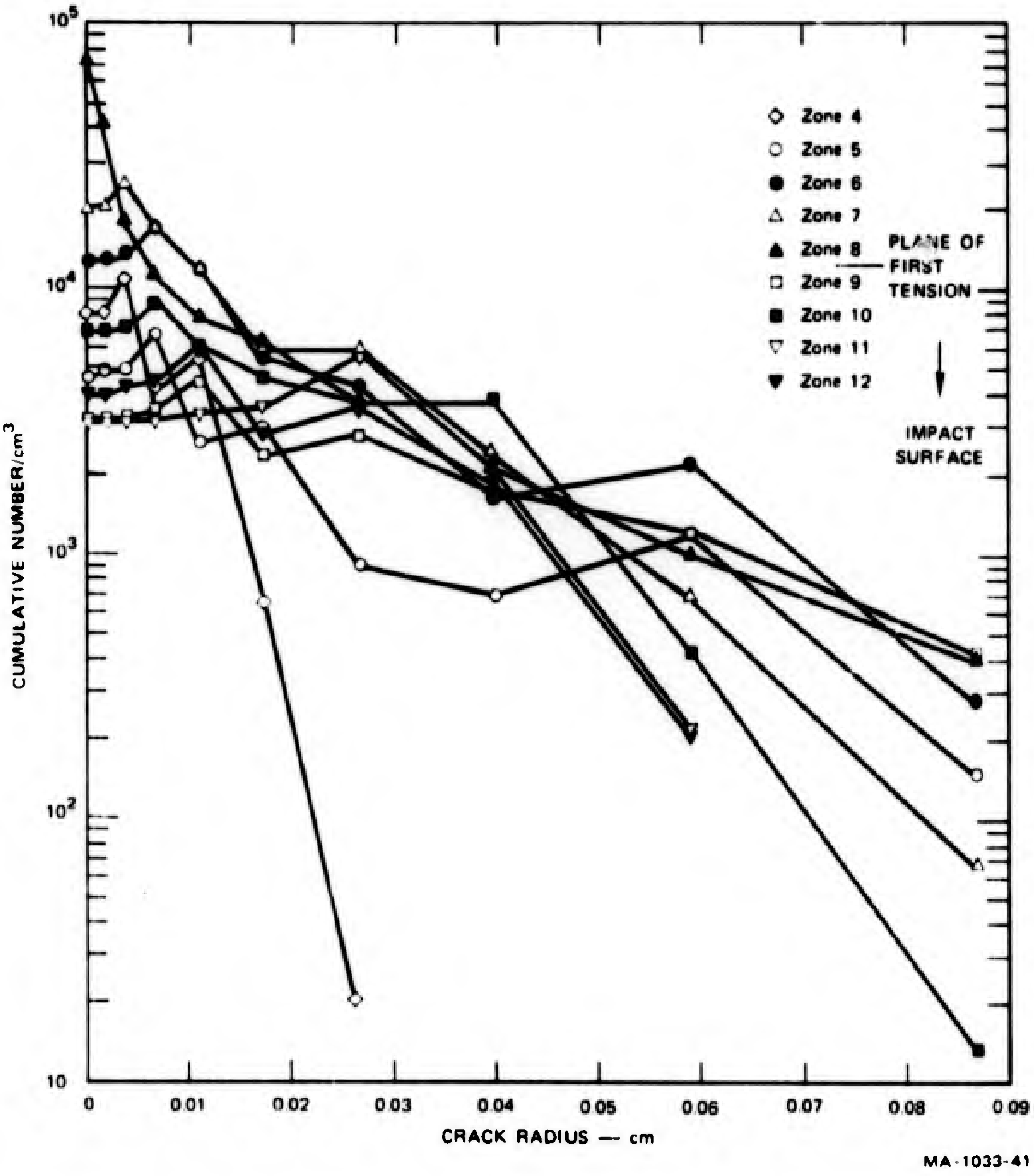

FIGURE 21 SIZE DISTRIBUTION OF CRACKS IN POLYCARBONATE SPECIMEN No. 6 AS A FUNCTION OF STRESS DURATION

The SRI PUFF[10] one-dimensional wave propagation computer code was used to compute the damage levels for polycarbonate, and the results were compared with the observed damage. We describe in the next section the brittle fracture model in SRI PUFF and show the correlation between the computed and observed damage.

The gas gun experiments on polyimide showed that this material cannot suffer significant shock damage and still remain intact. There exists a very small stress range between the stress necessary to cause damage to occur and that which will cause disintegration. An insufficient number of experiments were performed at stress levels within this range to do the detailed damage analysis done for polycarbonate. Instead the range is simply estimated from the measured impact velocities at which incipient damage and incipient disintegration occurred.

Since the constitutive relation of polyimide is not well established, the Hugoniot jump condition

$$\sigma = \rho_o U u$$

is used, where the shock velocity U is taken to be the measured elastic longitudinal wave velocity in the axial direction (Table II) and the particle velocity u is assumed to be half the impact velocity. Measured impact velocities of about 63 and 70 m/sec indicate that the threshold stress at load durations of about a microsecond for polyimide is about 1 kbar and that the stress at which disintegration begins is about 10% higher.

Model for Brittle Fracture

The basic calculational model for brittle fracture was developed during an earlier study of fracture in Armco iron.[2] The model has been recently modified to apply to fracture in beryllium.* The results of the modified model correlated well with damage observed in the polycarbonate.

---

* Monthly Progress Report No. 3, "Dynamic Fracture Criteria of Homogeneous Materials," Contract No. F26601-70-C-0070, By SRI to AFWL, November 15, 1971.

The brittle fracture model accounts for three aspects of the fracture process not normally taken into account; namely,

- Nucleation of cracks as a function of stress
- Growth of cracks as a function of stress, fracture toughness, and current crack size
- Decrease in strength and stress with increasing damage.

The model is incorporated into the BFRACT subroutine of SRI PUFF.[10] This routine also acts as a constitutive relation subroutine for portions of the material that are undergoing brittle fracture.

The nucleation rate was assumed to have the form

$$\dot{N} = \dot{N}_o \exp\left(\frac{\sigma-\sigma_{no}}{\sigma_1}\right) \tag{11}$$

where

σ_{no} is a threshold stress for nucleation

$\dot{N}_o$, σ_1 are constants.

This form of nucleation rate resembles the form given by Zhurkov[11] for the rate of breakage of atomic bonds. This same form has been found applicable to ductile fracture in 1145 aluminum and OFHC copper, and to brittle fracture in Armco iron.[2] The cracks are nucleated with a distribution of radii as follows:

$$\Delta N(R) = \Delta N_o e^{-R/R_1} \tag{12}$$

where

ΔN_o is the total number nucleated at a given time t per cm^3

$\Delta N(R)$ is the number nucleated with radii greater than R per cm^3 in the time between t and t + Δt

R_1 is a constant.

The growth of cracks has been treated by two possible functions. The first was the function of Dulaney and Brace[12] for propagation of a planar crack in elastic material

$$\frac{V_c}{V_t} = 1 - \frac{R^*}{R} \qquad R > R^* \tag{13}$$

where

V_c = growth velocity

V_t = terminal velocity

R = crack radius

R^* = critical crack radius.

The critical crack radius for a penny-shaped crack in a one-dimensional elastic tensile field is[13]

$$R^* = \frac{\pi E \gamma}{4\sigma^2 (1-\nu^2)} = \frac{\pi K_{Ic}^2}{4\sigma^2} \tag{14}$$

where

E = elastic modulus

γ = surface energy

σ = one-directional tensile stress applied at infinity

ν = Poisson's ratio

K_{Ic} = plane strain fracture toughness.

We note that Eq. (13) is for a planar crack in elastic material although our problem concerns a penny-shaped crack in plastic material. However, the expression was expected to give the correct form.

A second growth function was postulated to account for ductile behavior and viscosity-limited growth. This is the viscous growth law:

$$V_c = \frac{\sigma - \sigma_{go}}{4\eta} R \qquad (15)$$

where

σ_{go} = critical stress for growth according to Eq. (14) for $R = R^*$

η = material viscosity.

Calculations were made with both growth laws, but only those with Eq. (15) are presented since they correlated better with the experimental results. This decision is discussed in more detail later.

The constitutive relations for material with developing damage provide separate expressions for pressure and deviator stress. The expressions are continuous with those for undamaged material. The constitutive relations are based on treating the material as if it were composed of two components: solid and void. When a volume increase is applied to the material, there is some increase in crack volume by nucleation, growth, and elastic opening of the crack, and there is some change in specific volume of the solid material. The volume of a penny-shaped crack is taken from Irwin[14]

$$V = \frac{4\pi R^3 \sigma}{3E} \qquad (16)$$

Because plastic flow is not taken into account in this expression, the volume so obtained is a lower-bound estimate of the actual crack volume. Because the crack volume has been calculated according to elastic laws, it becomes zero when tensile stresses are removed.

The nominal stresses are obtained from the stresses in the solid material. The pressure in the solid is computed as follows for an increment in time and density:

$$\begin{aligned} p'_a &= \frac{PA}{1 - \alpha V_{cr} \rho} = p'_o - K \frac{V_s - V_{so}}{V_s} \\ &= \frac{PO}{1 - \alpha V_{cro} \rho_o} - K \frac{V_s - V_{so}}{V_s} \end{aligned} \qquad (17)$$

where

p_o' and p_a' are the computed initial and final pressures in the solid material

PO and PA are initial and final pressures on the gross section (values of interest for one-dimensional wave propagation)

ρ_o and ρ are initial and final densities of the gross material

V_{cro} and V_{cr} are initial and final total specific crack volumes

α is a dimensionless factor relating volume of damage to area of damage

K is the bulk modulus of the solid

V_{so} and V_s are initial and final specific volumes of the solid material.

The deviator stress is computed from

$$\Delta SD = \frac{4}{3} G \frac{\Delta V}{V} \tag{18}$$

up to yielding. The gross specific volume V is used here. The shear modulus G is reduced according to

$$G = G_o \left(1 - S_m \frac{V_{cr}}{V}\right) \tag{19}$$

where G_o is the shear modulus of solid material. S_m is a factor (about 2) from Mackenzie's[15] elastic analysis of porous material. Yielding occurs when the deviator stress reaches

$$SD = \frac{2}{3} Y \left(1 - \frac{V_{cr}}{V}\right) \tag{20}$$

The brittle fracture model in SRI PUFF requires six special parameters in an array labeled TSR (,). These are related to the parameters above as shown in Table VI.

With the brittle fracture routine in SRI PUFF, stress histories and damage can be computed for every cell undergoing fracture. The normal printout includes listings of stress histories at selected points, and histories of the number of cracks and the crack volume at those points. Periodically during the calculation, printouts are provided of the number of cracks of each size at each cell.

Table VI

FRACTURE PARAMETERS FOR POLYCARBONATE

Code Parameter	Name	Value*	Units
TSR(M,1) = $-1/4\eta$	Growth parameter	$-.0005$	$cm^2/dyn/sec$
TSR(M,2) = K_{Ic}	Fracture toughness	36×10^7	$dyn/cm^{3/2}$
TSR(M,3) = R_1	Nucleation radius	.002	cm
TSR(M,4) = $\dot{N}_o$	Nucleation rate	3.5×10^{10}	$No./sec\ cm^3$
TSR(M,5) = σ_{no}	Nucleation threshold	-1.67×10^9	dyn/cm^2
TSR(M,6) = σ_1	Nucleation parameter	-1.41×10^8	dyn/cm^2

* Stresses are chosen positive in compression.

Wave Propagation and Damage Calculations for Polycarbonate

To determine the fracture characteristics of any material, the following steps are taken:

- Perform several impact experiments to obtain different levels of damage. Quantify the damage and obtain damage distributions (number of cracks versus crack radius as a function of position in the sample).
- Compute the stress histories that would have occurred if there had been no damage. The tensile wave will normally appear as an approximately square pulse.

- Estimate the values of all six fracturing parameters considering the observed damage and the computed stress histories.
- Perform SRI PUFF calculations with the fracture model and obtain damage distributions.

The crack size distributions for polycarbonate (Experiments 5 and 6) are exhibited in Figures 20 and 21. In Experiment 7 very few cracks formed at a stress level which was probably near the threshold level for damage. The wave propagation computation for undamaged material indicated a duration of the tensile stress of 1.65 μsec and tensile stresses of 1.76, 1.66, and 1.60 kbar for impacts 5, 6, and 7. From these data, fracture parameters were estimated, and several iterative SRI PUFF calculations were performed. The fracture parameters used in the final calculations are given in Table VI The value of 36 x 10^7 dynes/cm^2 for the plane strain fracture toughness used in these calculations seems to be an underestimate (see Section IV),but subsequent calculations with a value of 58 x 10^7 dynes/cm^2 affected the results only slightly. The crack distributions computed for the impacts are shown in Figure 22 and 23. The cell numbers refer to the cells into which the target material was subdivided for the calculation. The peak damage occurred at PUFF calculational cell 23 near the middle of the target with lessening damage on either side (PUFF cells were approximately 0.03 cm wide).

These computed distributions may be directly compared with the experimental results in Figures 20 and 21. We note first that the slopes of the distributions in Figures 20 and 22 are similar, suggesting that the growth function is approximately correct. The slopes in Figure 23 are somewhat steeper than those in Figure 21. To compare the amplitudes and spatial distributions, intercepts at crack radii of 0.02 and 0.04 cm were plotted in Figures 24 and 25 as a function of depth within the target. These two figures show that the experimental damage is concentrated into a band between 0.32 and 0.40 cm from the impact plane and that there is some scatter in the data. The computed values have about the right

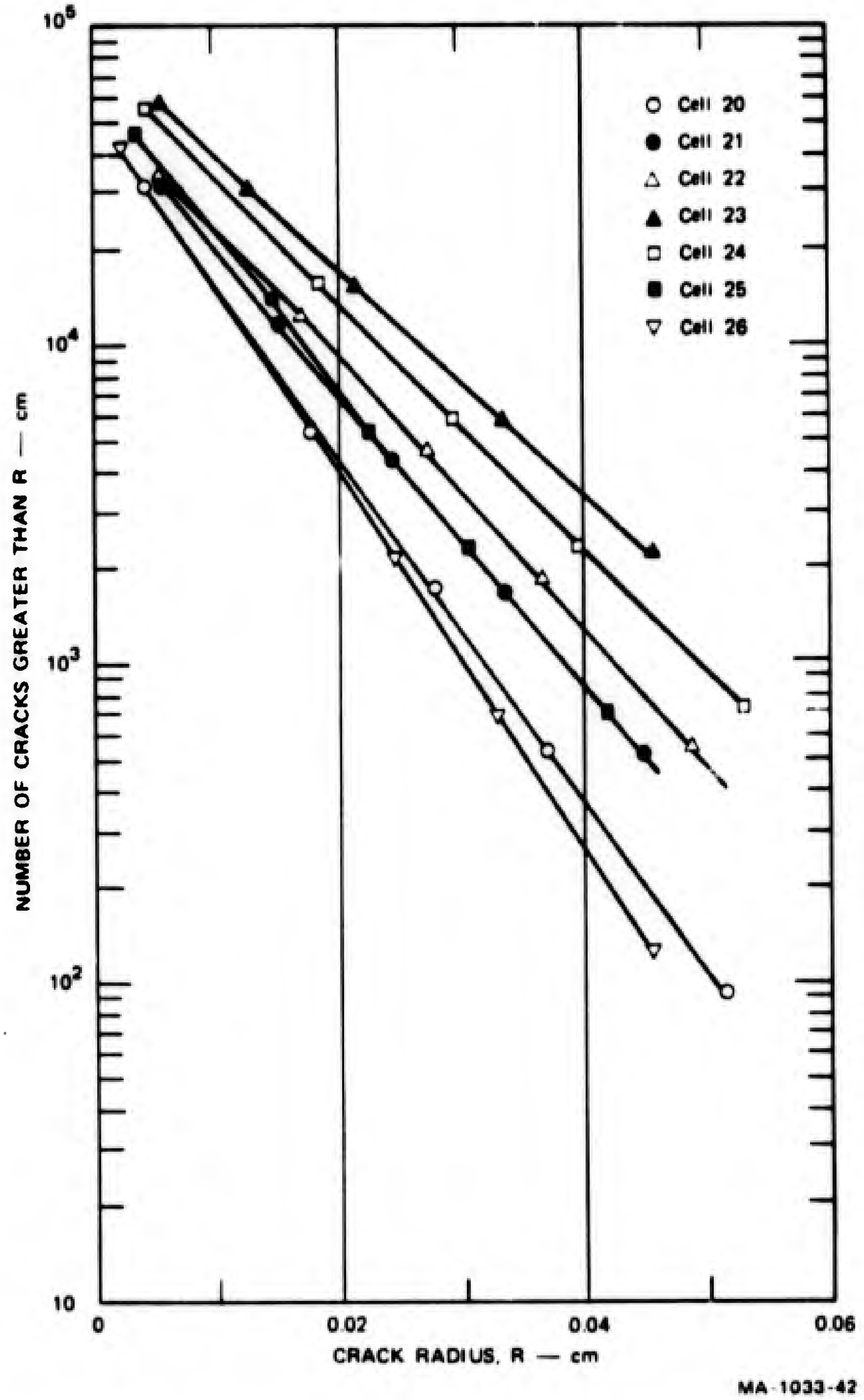

FIGURE 22 CALCULATED SIZE DISTRIBUTION OF CRACKS IN POLYCARBONATE SPECIMEN No. 5

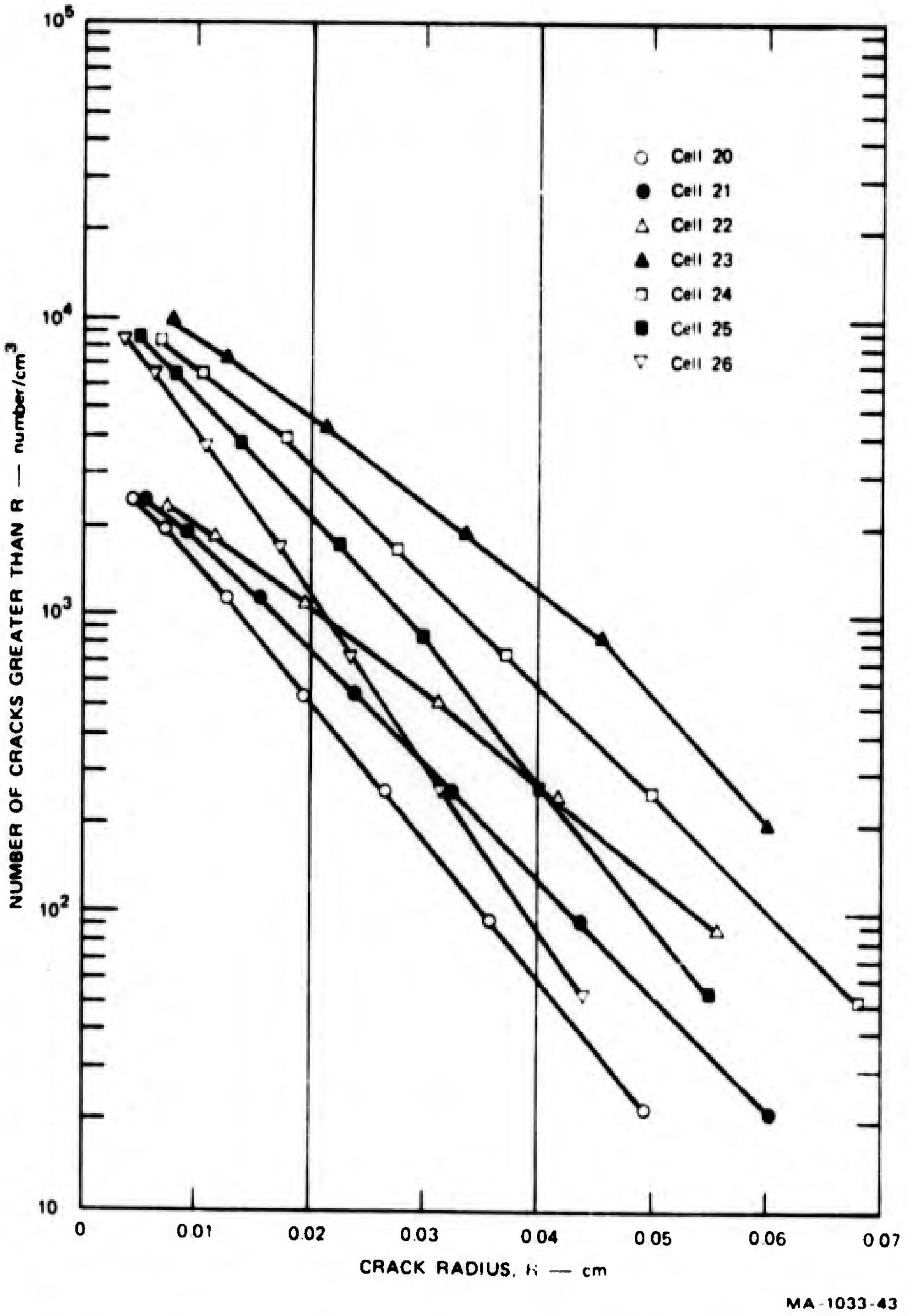

FIGURE 23 CALCULATED SIZE DISTRIBUTION OF CRACKS IN POLYCARBONATE SPECIMEN No. 6

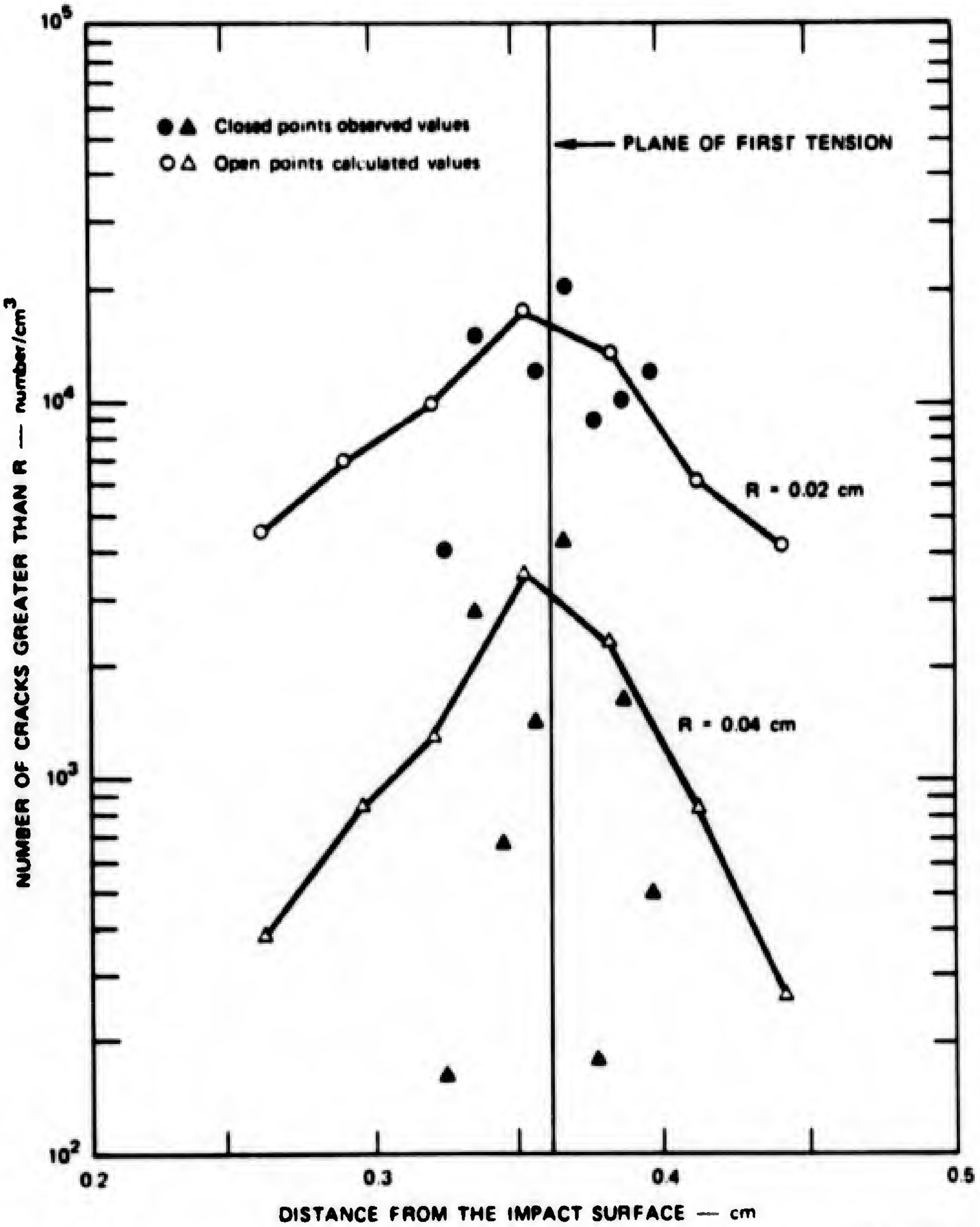

MA-1033-44

FIGURE 24 COMPARISON OF CALCULATED AND OBSERVED SPATIAL DISTRIBUTION OF DAMAGE IN POLYCARBONATE SPECIMEN No. 5 FOR TWO CRACK SIZES

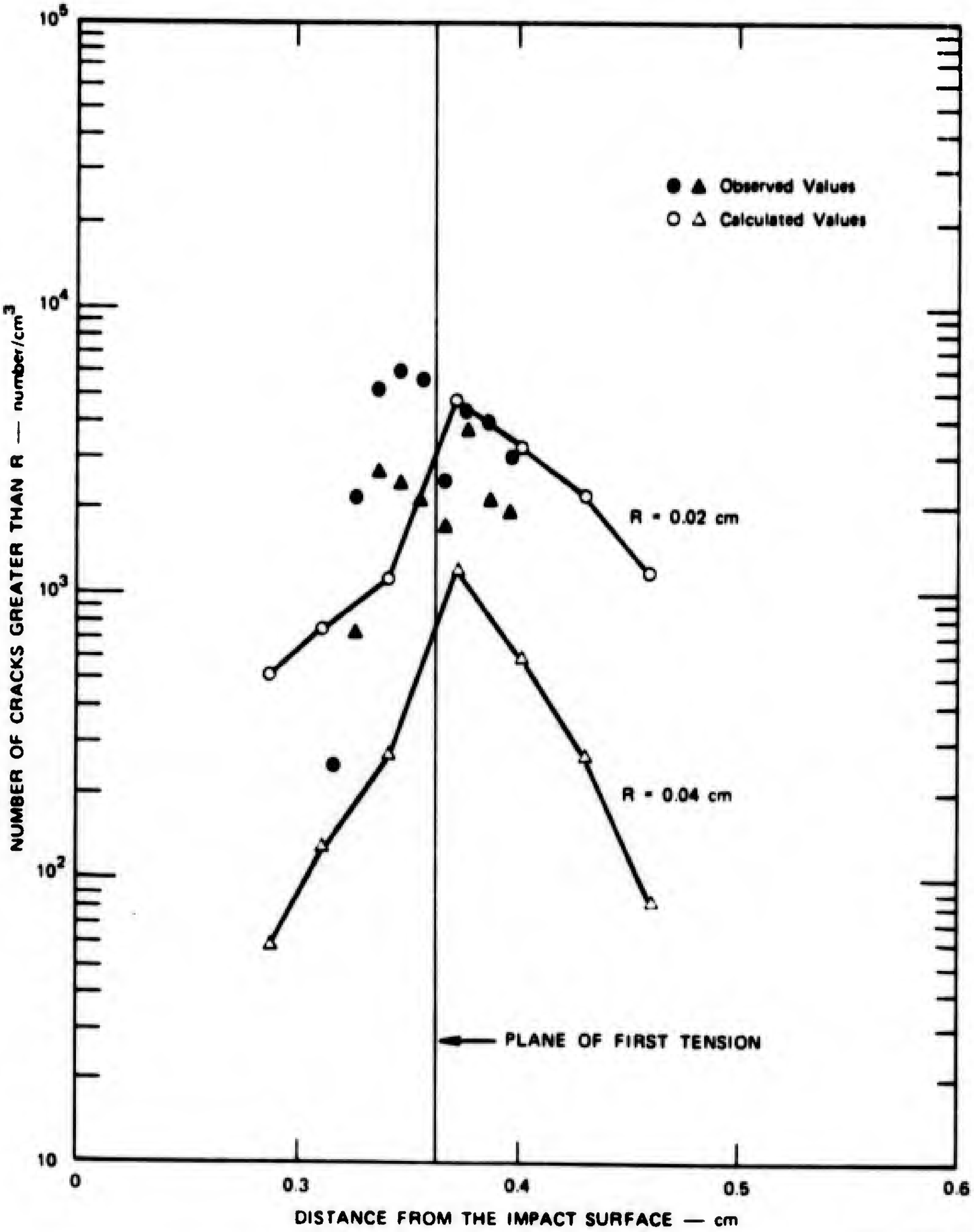

MA-1033-46

FIGURE 25 COMPARISON OF CALCULATED AND OBSERVED SPATIAL DISTRIBUTION OF DAMAGE IN POLYCARBONATE SPECIMEN No. 6 FOR TWO CRACK SIZES amplitude but have a wider and smoother distribution. While the computations appear to indicate the spall plane correctly in Figure 24, they are in error by about one cell width in Figure 25. Calculated results are not shown for Experiment 7, because of the low level of damage obtained there. Only one cell was undergoing fracture, but considerable damage occurred at that cell. This result compares at least qualitatively with the experimental observation that incipient damage is restricted to a very narrow band.

The general agreement between computed results and observed damage is considered very good. The correlation is much better than we obtained earlier with Armco iron.[2] The correlation with the shape of the N vs R distributions (Figs. 20 vs 22, and 21 vs 23) is especially intriguing, because it shows a viscous-dominated growth pattern. The conventional elastic growth law of Dulaney and Brace[12] which was used in the early fracture calculations indicated that all cracks achieved terminal velocity soon after nucleation. Therefore the computed distributions were nearly vertical lines at a radius corresponding to terminal velocity divided by tensile stress duration. From this comparison of results, it is clear that the viscous growth law is more appropriate than the elastic and therefore a viscous mechanism probably governs growth.

Isodamage Contours

For use of the present damage data in other applications, it is instructive to construct isodamage contours as a function of peak tensile stress and nominal stress duration (see Fig. 26). The ordinate in Figure 26 is the peak tensile stress from a calculation with damage and the abscissa is the duration of that peak tension. The contour lines indicate values of the damage parameter $\bar{A}$, where

$$\bar{A} = \frac{\pi}{V} \sum_i N_i R_i^2 \qquad (\mathrm{cm}^2/\mathrm{cm}^3)$$

Thus $\bar{A}$ is the total crack area (i.e., one half the total internal surface area) per unit volume of material. For brittle fracture this is a much more sensitive damage parameter than crack volume.

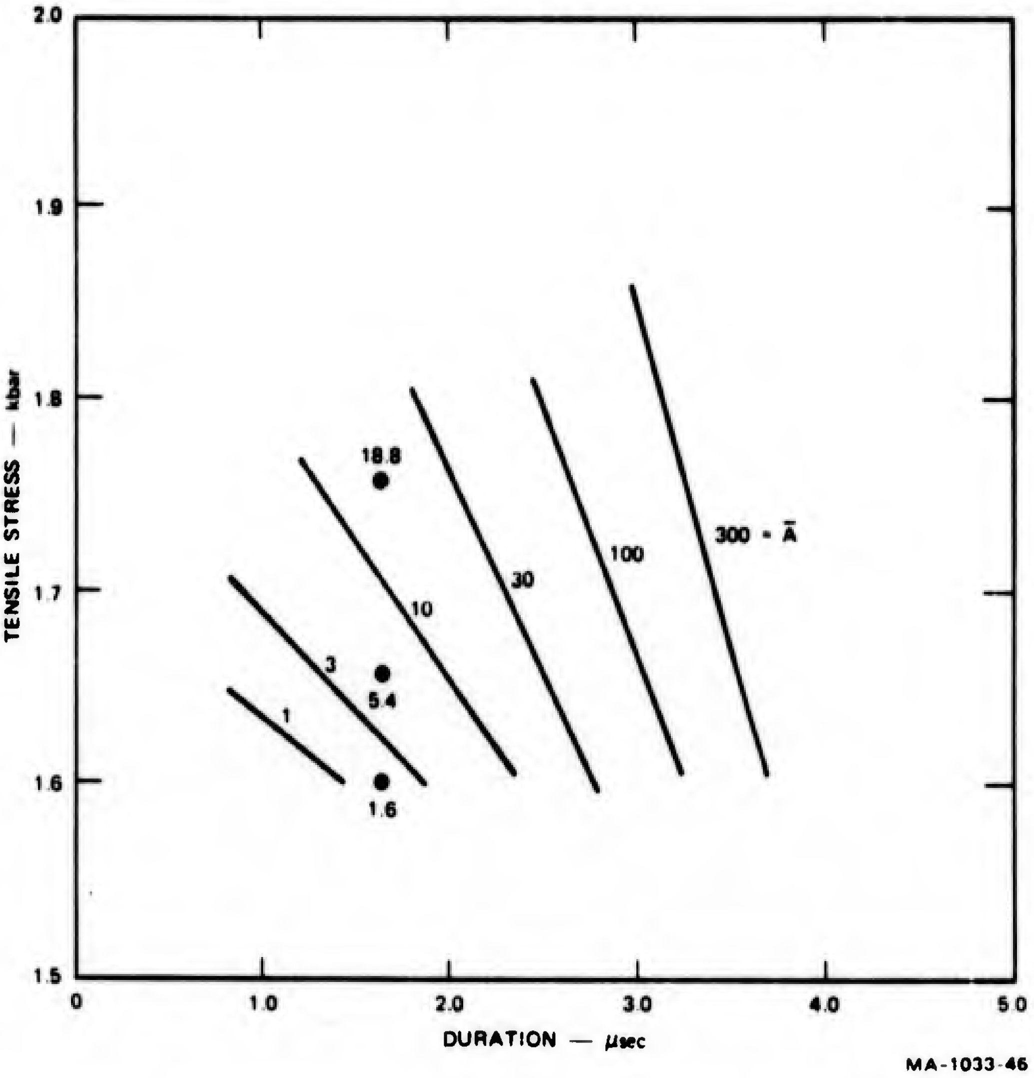

FIGURE 26 ESTIMATE OF ISODAMAGE CURVES FOR POLYCARBONATE AS A FUNCTION OF LOADING PARAMETERS

The contours were determined by performing impact calculations for several specimen thicknesses and interpolating to obtain the damage levels noted. The stress required to initiate damage is about 1.6 kbar. The contours come down to 1.6 kbar very steeply, probably because of the form of the nucleation function which has a sharp cutoff and is a strong function of stress above that cutoff. These isodamage curves should very gradually bend to the right to approach asymptotically the static strength (about 0.6 kbar) for long duration loadings. The present data points are also shown in Figure 26. This plot shows clearly that for an accurate construction of these isodamage curves experiments should be conducted at higher and lower stresses and with a range of stress durations (a range of flyer and target thicknesses).

Metallographic Observations

Flat-plate impact experiments subject specimens to a high amplitude compressive wave immediately before the tensile pulse occurs. It is conceivable that the passage of this compressive wave changes the material in some way so as to affect the fracture behavior. Therefore the flyer plates, which were manufactured from the specimen material and had seen only compression, were examined with an optical microscope and compared with virgin material to determine if the material had been changed in any way. In particular, evidence of crazing, incipient cracks or changes in texture or microstructure were sought. The absence of any such evidence leads us to assume that, at least at the low stress levels produced in this work, there is little effect on the fracture behavior of these materials from the initial compressive wave.

Fractographical features of individual cracks *in situ* could be studied at magnifications to 200X by focusing into the transparent polycarbonate specimens. The low damage shot shown in Figure 27, in which crack interaction was at a minimum, was especially suited for microscopic investigations of the fracture process.

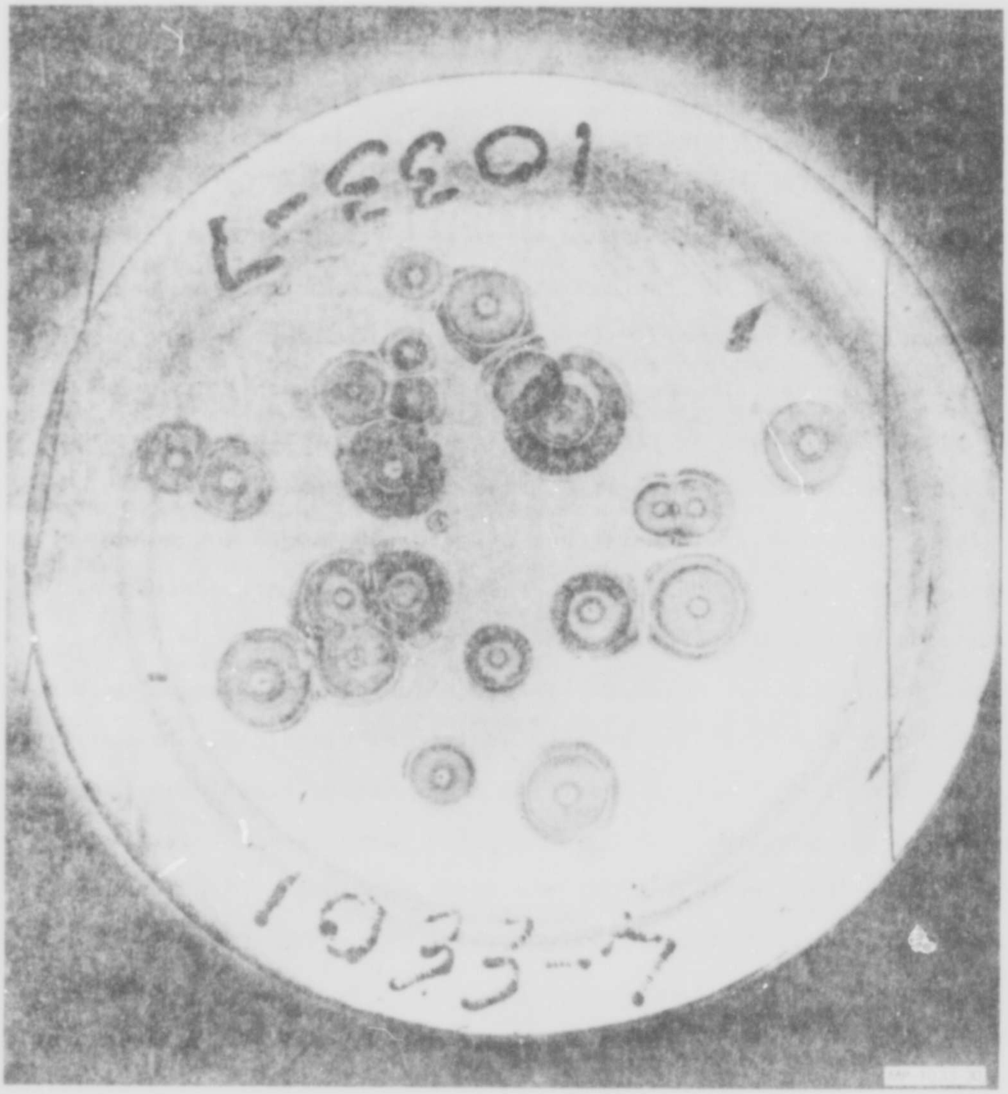

FIGURE 27 INTERNAL CRACKS IN POLYCARBONATE PRODUCED BY A SHORT-LIVED TENSILE PULSE

Individual cracks were circular and penny-shaped and lay on planes normal to the impact direction. Features common to all cracks were central "points" surrounded by a rather smooth area which in turn was encompassed by an annulus of rough surface. It is tempting to follow common practice[16,17] and associate the point at the center with the classical nucleation flaw, the mirror region with slow accelerating crack growth, and the rough hackle with crack growth at maximum velocity. The relative constancy of the diameters of the central point and the smooth annulus are in accord with this interpretation, since a nucleating heterogeneity is usually required to reach a certain critical size before crack growth can occur, and it is usually felt that a crack must accelerate for a certain distance before it attains maximum speed.

There are, however, usually one or more additional concentric rings outside the hackle. These may be caused by one or more additional propagation phases of the cracks under damped reverberations of the original tensile pulse. Credence is given to this speculation by the fact that only the large cracks have additional rings; this is consistent with the concept of fracture mechanics that smaller flaws require larger stresses for propagation. That is, smaller flaws show no additional rings because the damped reverberated stresses are not large enough to cause propagation, whereas for larger flaws they are.

A peculiar observation is that 5 cracks (and parts of 3 others) near the center of the specimen show marked roughness in an outer annulus. Since the roughness is confined to the outer rings, it is considered to occur during one of the stress reverberations, and the fact that the phenomenon affects cracks only near the specimen center suggests that a reverberation stress wave running radially is involved.

In light of the results of Sommer[18] who produced a similar hackle in glass rods by fracturing them in tension with superimposed torsion, it is conceivable that the roughness results from repropagation under mixed mode loading produced by the interaction of waves reflected from the flat sides and those running in from the periphery.

A further observation perhaps reveals something of the fracture process in polycarbonate as well as in polymers generally. Tiny flaws very much reminiscent of conceivable fracture nuclei have been observed outside the crack tip periphery of small cracks, (Figure 28). This observation is in accord with several theories of the fracture process which maintain that propagation proceeds by continued nucleation of tiny flaws ahead of the dominant crack tip under the action of the magnified stress field which exists there[19] followed by the coalescence of these with the main crack. The second step is nicely illustrated by Figure 29 which shows a larger crack in the same specimen that has apparently engulfed several such nuclei as it expanded. The existence of characteristic hyperbolae resulting from this interaction is well documented in many plastics fractured in quasi-static tests.

An additional microscopic feature of the fracture surfaces is the one-, two-, or three-pronged spikes which extend out from the nucleus radially through the mirror in many of the cracks. These probably are formed when nucleating heterogeneities lie on planes other than the plane normal to the maximum tension, for then the crack starts to grow on two or more planes intersecting the heterogeneity. The spikes are the lines of coalescence where the various sections of the crack merge.

Metallographic observations of shock-damaged polyimide were made by the usual procedure used for opaque materials of examining the exposed fracture surfaces. The surfaces were much smoother and exhibited significantly less evidence of tearing, but the overall fractographic features were much like those described above for polycarbonate. As in polycarbonate, circular, penny-shaped cracks normal to the impact direction were found which, having gone through the coalescence stage, ended up in dish-shaped configuration. A distinguishing feature was that vivid colors were present on the nominally dark brown polyimide fracture surface. Bright red and yellow thread-like markings radiated outward from the fracture centers, and patches of red often delineated the concentric ring pattern.

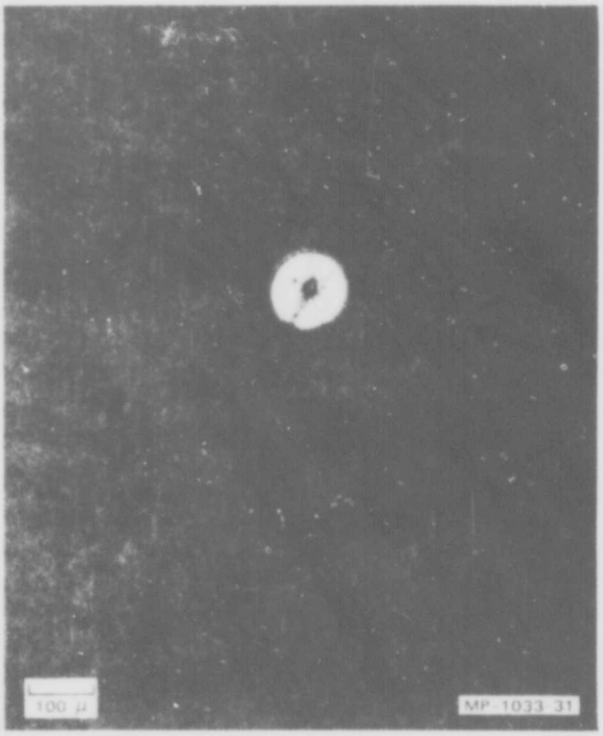

FIGURE 28 TINY CRACK-LIKE FLAWS ABOUT THE PERIPHERY OF A SHOCK-INDUCED INTERNAL CRACK IN POLYCARBONATE

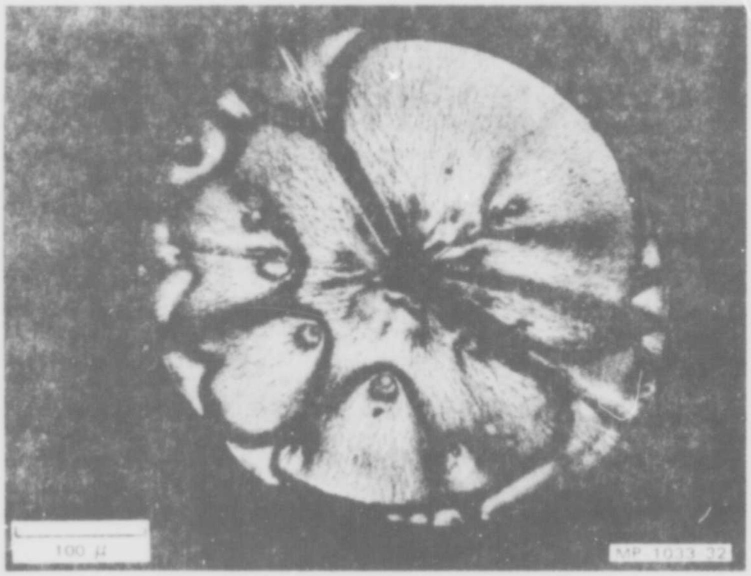

FIGURE 29 TINY CRACK-LIKE FLAWS WHICH HAVE BEEN ENGULFED BY A GROWING CRACK RESULTING IN HYPERBOLIC MARKINGS ON THE FRACTURE SURFACE

IV THE MECHANISM OF FRACTURE IN POLYMERS

The nucleation and growth rate functions, as summarized in Table IV for polycarbonate, can be used to predict shock damage regardless of whether or not the microscopic processes that govern these functions are completely understood. Nevertheless meaningful fracture criteria should be based on the actual physical processes by which damage occurs. Thus it is important to study in detail the sequence of events which occurs in the polymers during the loading cycle to produce the damage.

The fracture mechanism was studied mainly by post-mortem examination of the fracture damage using optical and scanning electron microscopy. These investigations were greatly facilitated by the transparency of polycarbonate, which permitted almost casual observations of in situ internal cracks and thereby allowed us to draw some interesting and important conclusions. Examination of the fracture surfaces of opaque polyimide specimens strongly indicates that polyimide, although considerably more brittle than polycarbonate, fractures in a manner very similar to polycarbonate, and that, therefore, the fracture mechanism which we propose in this report is very probably the mechanism by which fracture occurs in the entire class of polymeric materials.

On the basis of metallographic observations on impacted and damaged polycarbonate specimens, it appears that the fracture process may be divided into four stages: crack nucleation, crack growth, crack coalescence, and separation into two or more parts. To study crack nucleation effectively, we must first examine the as-received material, looking in particular for preexisting crack-like defects and other heterogeneities which could conceivably act as stress raisers or zones of weakness. A very short stress-pulse of sufficient intensity to activate several cracks but of such short duration that large amounts of crack growth cannot occur is useful in revealing sites that are effective crack starters. Stress pulses of increasing duration allow fracture to proceed to the next stages, and crack growth and coalescence can be studied by subsequent fractographic examination.

Since fracture damage can be correlated with some function of stress and time-at-stress, progress of the fracture process can be controlled by controlling the stress level at constant stress duration, or alternatively by controlling stress duration at constant stress. Both methods were used in this work to study the fracture mechanism in detail. The stress duration at nominally constant load varied within individual specimens and the stress at constant stress duration was varied from specimen to specimen by varying the impact velocity.

Crack Nucleation

We ascertained by focusing into polycarbonate specimens with an optical microscope at 200X that polycarbonate has internal preexisting defects of essentially two types; namely, a rather dense and homogeneous dispersion of roughly spherical bubble-like voids approximately one micron in diameter, and a much less dense, randomly dispersed population of sharper, crack-like defects having an average diameter of about 20 μ (Figure 30). The shape of the former type suggests that they may have been caused by trapped moisture or gases originally dissolved in the fluid material before molding but which have come out of solution and precipitated during the cooling process. The latter type likely results from inclusions of foreign material, such as dust particles or traces of thermally degraded material or other resins from the mold walls.

Shock damage will initiate preferentially at the crack-like defects. Because of their larger size and sharper profile, the stress is concentrated more effectively and the defects become unstable at lower nominal stresses than smaller spherical bubbles; hence, at stress levels of the order of the threshold level, they control the initiation phase of the fracture process.

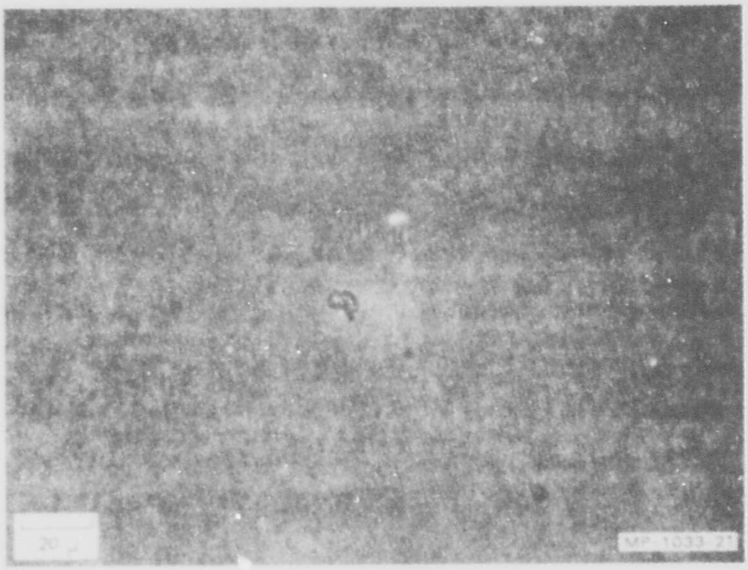

FIGURE 30 OPTICAL MICROGRAPH SHOWING THE TWO TYPES OF DEFECTS TO BE FOUND IN THE INTERIOR OF INJECTION-MOLDED POLYCARBONATE SHEET

However at sufficiently high stresses, the small bubbles will become important in crack initiation, for then both defect types can be activated with more or less equal facility. Then, because of the larger number of bubbles, they would control the initiation phase of the fracture process.

Scanning electron microscope techniques were used to examine the nucleation sites on brittle fracture surfaces of polyimide (Figure 31). Measurements of a large number of nuclei indicated that the maximum size of preexisting flaws was essentially the same as found in polycarbonate; namely, 20μ. Close-up views (to 50,000X) of the centers of cracks failed to reveal any consistent tangible inclusion. In the majority of cases, a cavity or a roughened surface was found at the center of cracks in

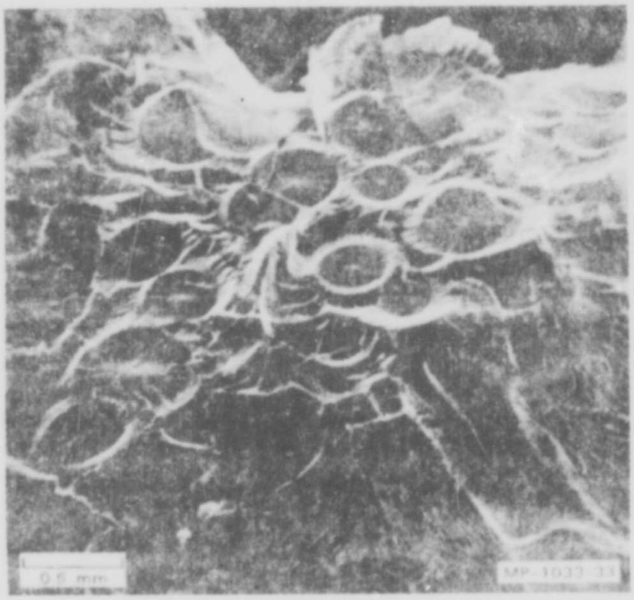

FIGURE 31 LOW MAGNIFICATION VIEW OF A SECTION OF A FRACTURE SURFACE IN SHOCK-LOADED POLYIMIDE

polyimide as shown in Figures 32 through 35. This is in accordance with the *in situ* observations of preexisting defects in polycarbonate and suggests that the same type of preexisting defect structure exists in polyimide, i.e., the rough fracture centers were the crack-like defects and the cavities were preexisting bubbles.

On rare occasions inclusions were found at crack centers. One such case is shown in Figure 36. A nondispersive x-ray analysis of the smooth-sided object revealed that the inclusion is a hydrocarbon.

Estimate of the Critical Stress Intensity Factor Under Shock Loading

According to concepts of modern fracture mechanics, there exists a number K_{Ic} which describes the resistance of a material to catastrophic brittle fracture under quasi-static loading. This number is considered to be a material property dependent only on testing temperature and strain rate and independent of specimen geometry. Moreover, the number

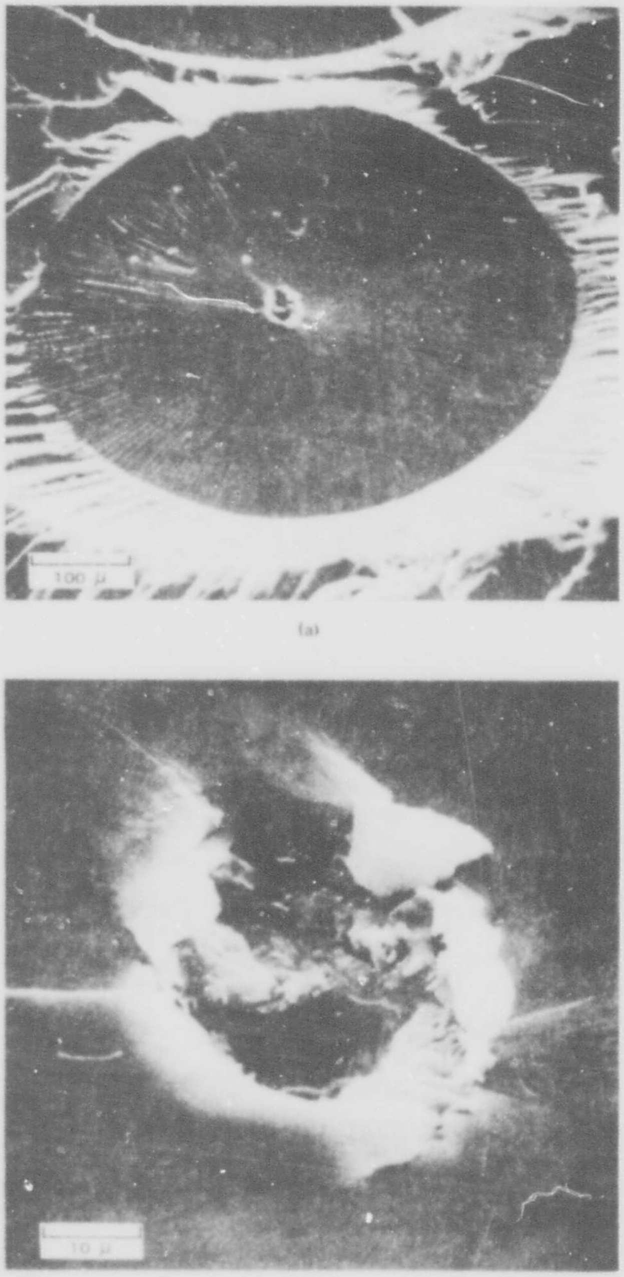

(a)

MP-1033-34

(b)

FIGURE 32 A CAVITY-TYPE NUCLEATION SITE IN POLYIMIDE

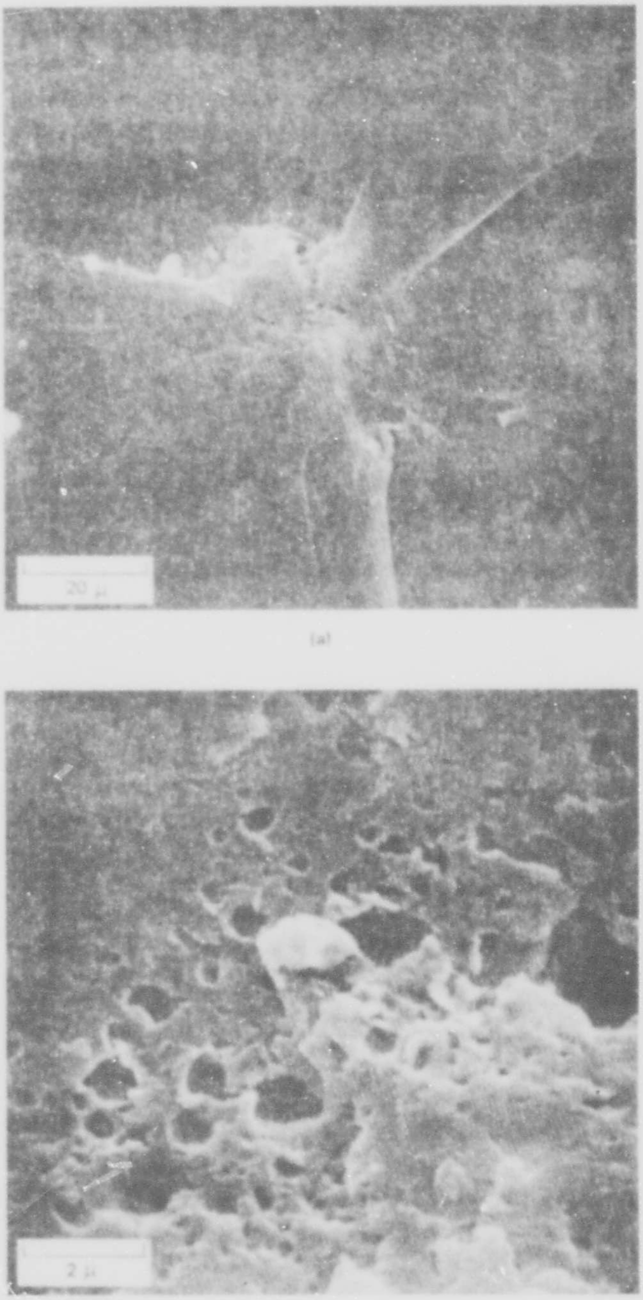

(a)

MP-1033-22

(b)

FIGURE 33 A POROUS AREA IN POLYIMIDE THAT SERVED AS A CRACK NUCLEATION SITE

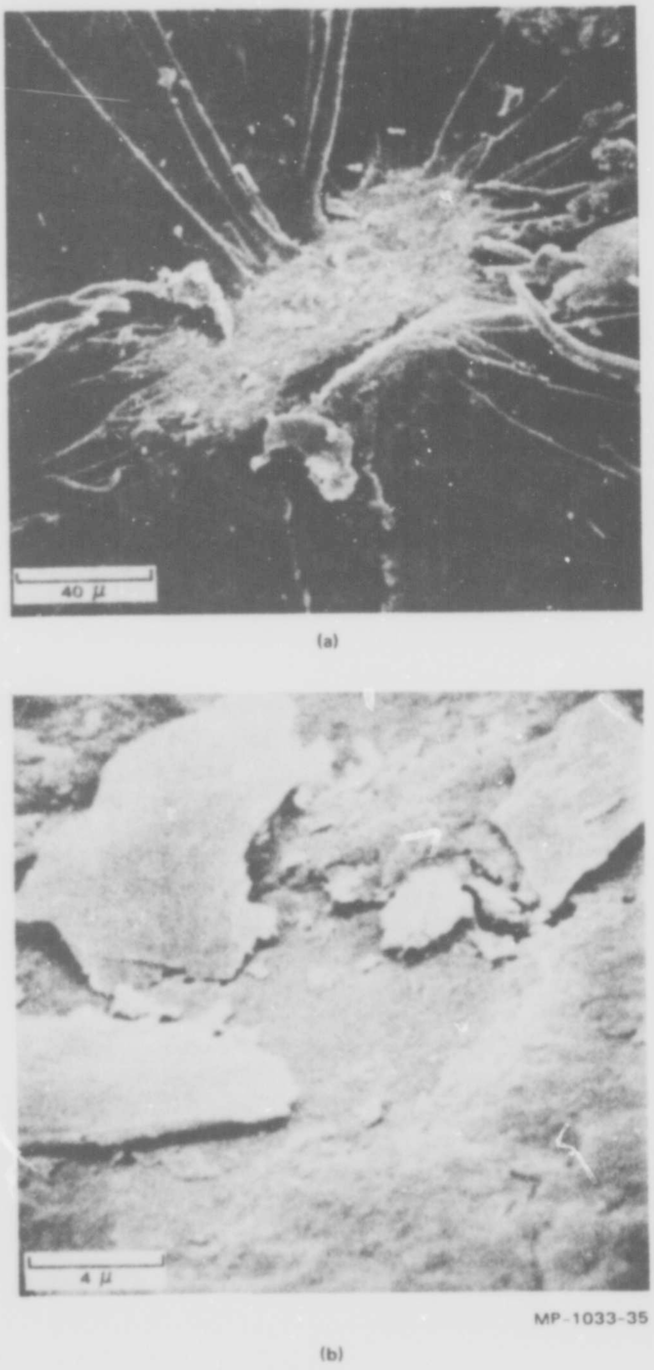

FIGURE 34 ROUGH AREA IN POLYIMIDE WHERE AN INTERNAL CRACK WAS INITIATED UNDER SHOCK LOADING

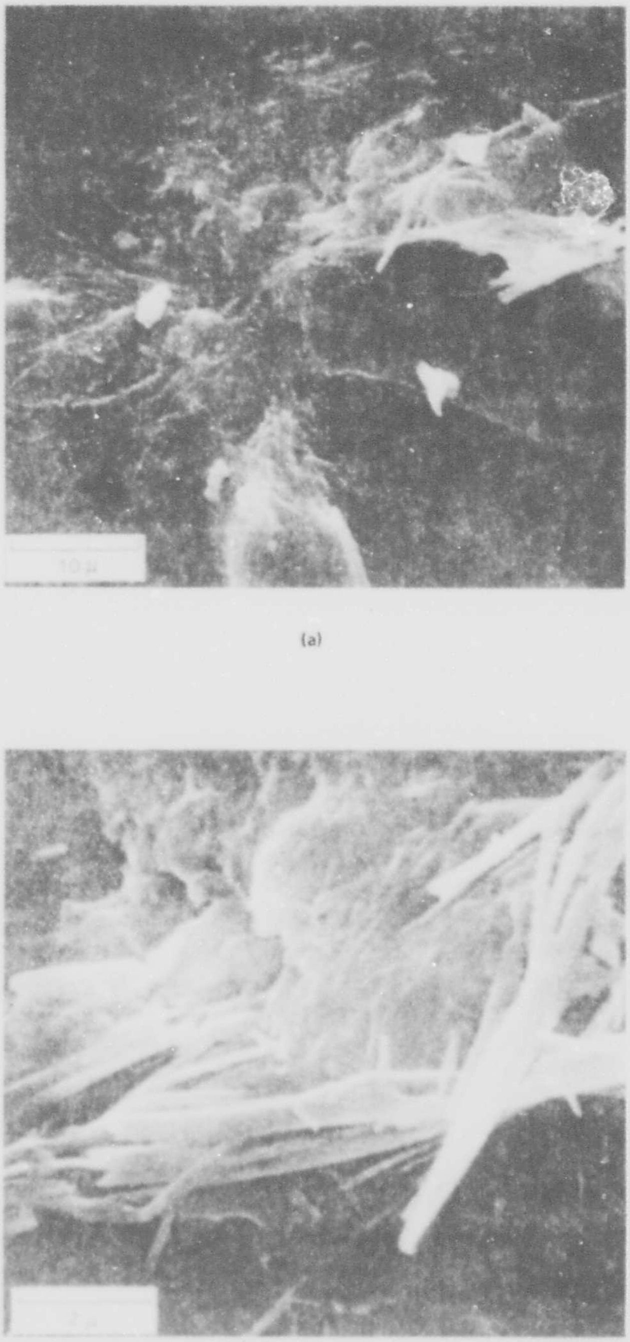

(a)

(b)

MP-1033-23

FIGURE 35 FIBROUS AREA IN POLYIMIDE WHERE AN INTERNAL CRACK WAS INITIATED UNDER SHOCK LOADING

FIGURE 36 SMOOTH-SIDED PARTICLE FOUND AT THE CENTER OF A CRACK IN POLYMIDE

can be used in design calculations and is thus much like the yield strength.

It is interesting to estimate the critical stress intensities of polycarbonate and polyimide under the shock-wave loading and uniaxial strain conditions which existed in these experiments. Since the cracks form before unloading waves can run in from the sides, the specimen behaves as if it were infinitely wide. The three-dimensional elastic solution for a penny-shaped crack in an infinite medium is[13]

$$K_{Ic} = \frac{2\sigma_f \sqrt{c}}{\sqrt{\pi}} \qquad (21)$$

where σ_f is the stress required to propagate a crack of half-length c. Substituting into this relation the measured threshold stresses and preexisting crack sizes, values of the critical stress intensity under dynamic conditions in polycarbonate and polyimide are 60 and 30 $kg/cm^{3/2}$, respectively.

Because of the uncertainties in the value of the nucleating defect sizes and the assumption that the static relation[15] holds under shock conditions, these fracture toughness numbers cannot be considered accurate. Nevertheless, the comparative toughness of polycarbonate and polyimide under these shock-loaded conditions is approximately indicated and comparison with the measured K_{Ic} of PMMA[20,21] of about 50 $kg/cm^{3/2}$ indicates that the values for polycarbonate and polyimide are of the right order of magnitude.

The mirror regions on the fracture surfaces of both polymers investigated in this work were remarkably circular and well defined. Since they are so prominent and hence easily measured, the establishment of a relationship linking mirror size with some mechanical or physical property of the polymer would be most welcome.

For example, in glass under uniaxial tension the breaking stress is approximately proportional to the square root of the mirror radius.[22,23]

$$\sigma = m\, r^{-\frac{1}{2}} \qquad (22)$$

If a similar relationship holds for polymers under the present experimental conditions and the constant m can be determined, it may be possible to determine dynamic fracture toughness from straightforward fractographic measurements on the spalled surfaces. The critical stress intensity for a penny-shaped crack in an infinite solid is given by Eq.(21). Assuming this relation holds for dynamic loading conditions and combining with Eq.(22) we obtain

$$K_{Is} = 2m\left(\frac{c}{\pi r}\right)^{\frac{1}{2}} \qquad (23)$$

where K_{Is} is the fracture toughness under these specical conditions of uniaxial strain and shock loading. This expression would allow fracture toughness determinations, normally an expensive and time-consuming task, to be made by making simple measurements of features on the fracture surface. The size of the nucleating flaw 2c can be measured with a scanning electron microscope.

In attempting to determine K_{Is} values it was found that the proportionality coefficient was a function of the impact stress. A determination of this function would be interesting but was not attempted in the present work. Order of magnitude values of m for polycarbonate and polyimide are 600 kg/cm and 300 kg/cm, respectively. These values yielded K_{Is} values of 150 kg/cm$^{3/2}$ for polycarbonate and 90 kg/cm$^{3/2}$ for polyimide and appear to overestimate the toughness by a factor of 2 or 3.

Crack Growth

Considerable information concerning the growth of cracks in polymers was obtained from a single impact experiment in polycarbonate in which the stress was only slightly greater than the threshold level. The low stress level activated only a limited number of microdefects (about 48) which then could grow with minimal interference from neighboring cracks. Hence, the growth of individual cracks and also the coalescence of pairs or larger groups could be studied at various stages of development and, perhaps more importantly, in the absence of any influences of competing fracture processes in the immediate vicinity.

Figure 27 is a micrograph taken in the impact direction of this polycarbonate target specimen showing the incipient spall damage in the form of distinguishable, individual, penny-shaped cracks within the specimen. Crack growth took place on planes that were perpendicular, with very little deviation, to the impact direction. Among the markings on the crack surface are several concentric rings, which are thought to be formed by changes in the growth velocity and thereby imply that the cracks grow radially outward. Several such rings are typically seen on any one crack surface, suggesting that the crack growth rate does not remain constant, but in fact accelerates and decelerates several times. The cracks may even arrest, and then repropagate under subsequent stress reverberations. Interpretation of the ring patterns on crack surfaces is an intriguing problem. The growth history of the crack pictured in Figure 37a, for example, might have been as follows: at the beginning of the first tensile pulse, a planar crack was initiated at the site of the irregular inclusion at the center of the photo. The crack expanded radially at a low velocity and very gradually accelerated until its size was such that the Griffith-Irwin condition[24] was fulfilled, i.e., the crack radius was such that

$$\sigma_{app}\sqrt{c} \geq \frac{(\pi)^{\frac{1}{2}}}{2} K_{Ic} \qquad (24)$$

where σ_{app} is the tensile stress in the pulse and K_{Ic} is the plane strain fracture toughness of polycarbonate for the strain rate of the experiment. At this size the crack accelerates very rapidly to run at a high velocity approaching that of Rayleigh waves in the material. But suddenly the stress falls to zero as unloading waves run in from the surfaces. The crack stops abruptly and is stationary as the material enters a compression cycle. But as the material experiences the first tensile reverberation, the crack may again accelerate rapidly and

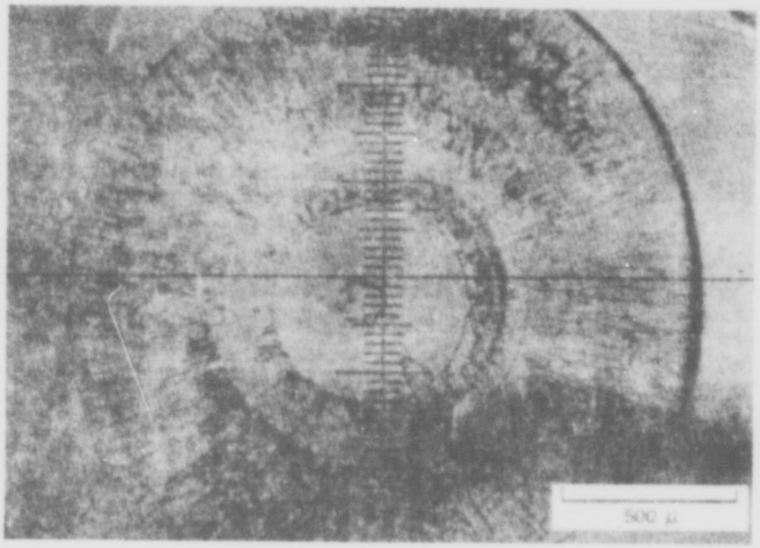

FIGURE 37a INTERNAL PENNY-SHAPED CRACK IN POLYCARBONATE PRODUCED UNDER SHOCK LOADING SHOWING CONCENTRIC GROWTH RINGS

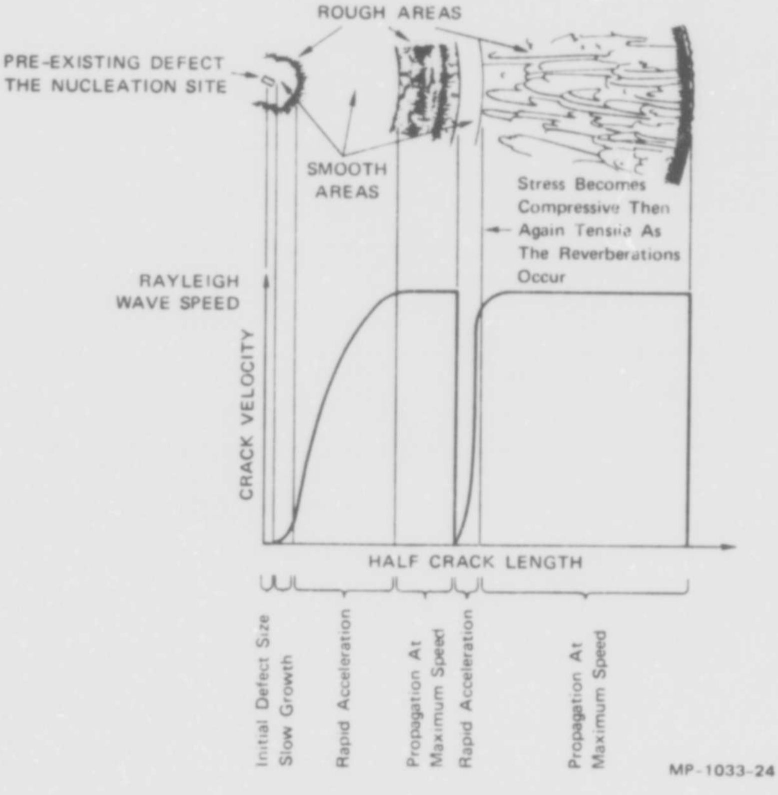

FIGURE 37b SCHEMATIC DEPICTION AND SUGGESTED VELOCITY HISTORY FOR THE CRACK SHOWN IN (a)

propagate at near maximum velocity if the size of the crack and the amplitude of the second tensile wave satisfy Eq. (24). Continued ringing of the stress waves could in this way produce further intermittent growth of cracks. This proposed growth history of a crack is illustrated in Figure 37b.

Crack Coalescence

The sequence of events leading to crack coalescence is depicted schematically in Figure 38. Crack tips of two neighboring cracks, radially expanding on parallel planes, will eventually approach each other to the point where the concentrated stress fields associated with them overlap. Therefore, the material between the two cracks is subjected to magnified stresses, and because of the proximity of two free surfaces (on which the stress has fallen to zero) the direction of the maximum tensile stress is altered. Now since crack growth in an isotropic material usually occurs on planes normal to the maximum tensile stress direction, both cracks tend to leave the nominal spall plane and turn into one another. This process, carried to completion so that the two cracks join up, is called crack coalescence, and is an important stage in the fracture process.

Cracks which had reached the coalescence stage were no longer penny-shaped, but rather, dish-shaped. The crack profiles on sectioned surfaces are shown in Figures 14 and 15 and depicted schematically in Figure 38d. A basic difference was observed in the degree of coalescence of polycarbonate and polyimide; namely, a high percentage of neighboring cracks in polyimide coalesced completely whereas the crack tips in polycarbonate, while strongly interacting and turning toward each other, very seldom joined up. This behavior probably results from the greater ductility of polycarbonate and is reflected in the difference in disintegration stress. Specifically, as the crack tips approach each other,

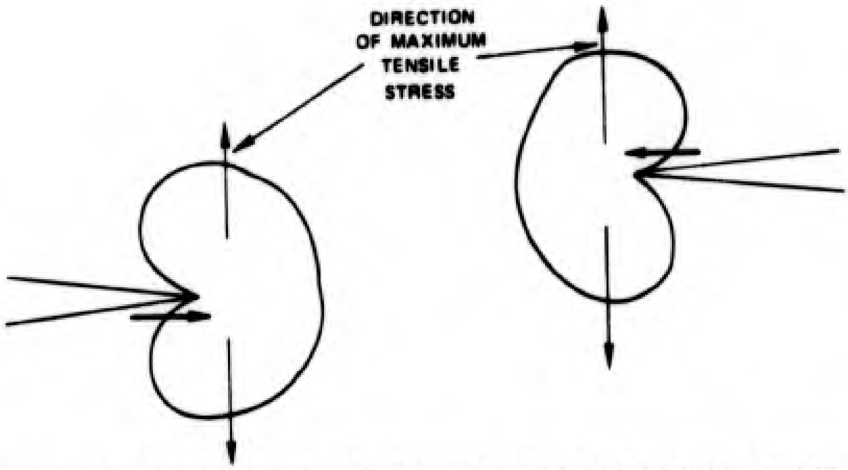

(a) TWO PENNY-SHAPED CRACKS LYING ON PARALLEL PLANES AND EXPANDING TOWARD EACH OTHER. UNDISTURBED STRESS FIELDS ARE SHOWN SCHEMATICALLY.

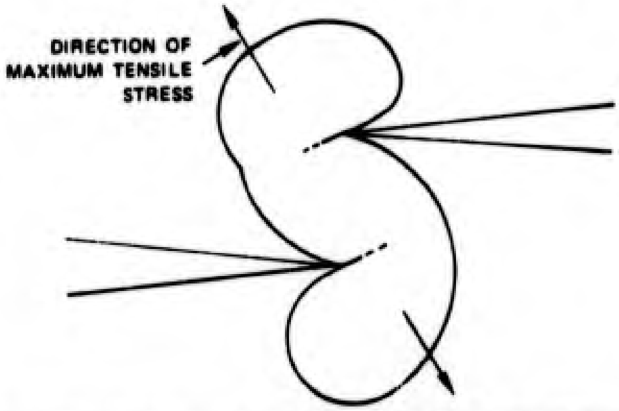

(b) CRACK TIPS HAVE MOVED INTO EACH OTHER'S STRESS FIELDS. DIRECTION OF THE MAXIMUM TENSILE STRESS HAS CHANGED. CRACK TIPS BEGIN TO TURN TOWARD EACH OTHER.

(c) STRESS IS REMOVED AND CRACKS HAVE STOPPED. CRACKS WHICH WERE PENNY-SHAPED IN THEIR EARLY STAGES OF FORMATION ARE NOW DISH-SHAPED.

(d) DAMAGE CONSISTS OF CRACKS HAVING ONE OF TWO SHAPES

MA-1033-25

FIGURE 38 SCHEMATIC DEPICTION OF THE SEQUENCE OF EVENTS LEADING TO CRACK COALESCENCE IN AMORPHOUS POLYMERS the cross section of the material supporting the stress becomes increasingly smaller. It is well known that deformability increases with decreasing size, and thus the intact material between the coalescing cracks can continue to deform, and thereby continue to relieve the stress. When the stresses fall below a certain level, the crack tips stop advancing, so that through the ability to relieve stresses by plastic flow, crack coalescence is inhibited, and separation of the specimen into pieces (the fourth and final stage of the fracture mechanism) is prevented. This is usually not the case for the brittle polyimide, whose ability to flow plastically is insufficient, even in small sections, to reduce the stresses to a point where fracture must arrest. Hence, the fracture process usually goes beyond the coalescence stage and proceeds to the final stage of specimen disintegration.

The micrograph of Figure 39 indicates qualitatively the magnitude of the concentrated stresses in the material between two converging crack tips as well as the thin-section enhanced ductility of polycarbonate. The conditions are such that voids can nucleate and grow.

Separation of the Specimen into Pieces

The final stage of the fracture process, separation of the specimen into two or more parts, could only be studied in polyimide, since none of the polycarbonate specimens reached this stage. Even the gaged polycarbonate shot, which was impacted at twice the stress necessary to initiate damage, although heavily damaged, (Figure 40) remained intact and retained considerable strength. Coalescence of spall cracks in polyimide, on the other hand, occurred with relative ease and usually resulted in a continuous pock-marked internal surface extending to about 1/4-in. of the specimen periphery, (Figure 41). Spall cracking never occurred within this outer annulus of the specimen because unloading waves running in from the sides prevented the tensile stresses

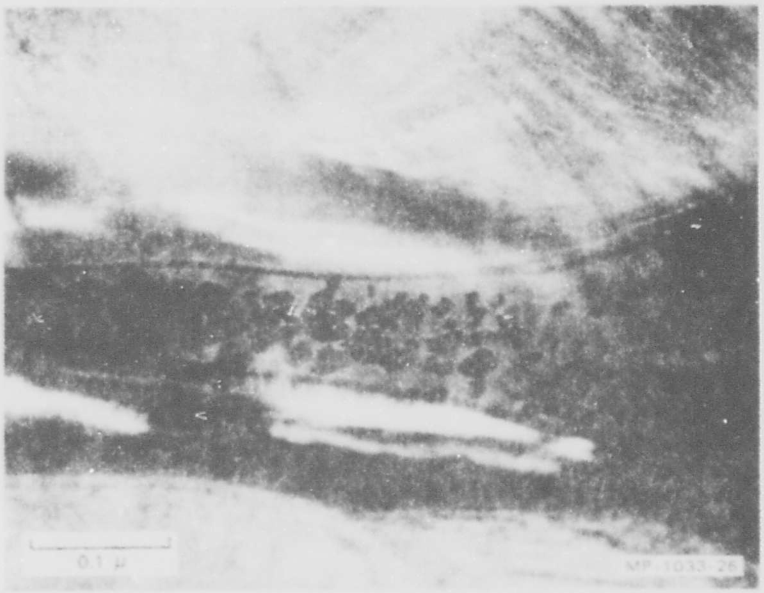

FIGURE 39 VOIDS THAT NUCLEATED AND GREW VISCOUSLY UNDER THE MAGNIFIED STRESS FIELD EXISTING BETWEEN TWO CONVERGING CRACK TIPS

from reaching critical values there. Hence spall cracks alone were not enough to disintegrate the specimen, since they did not reach the specimen surface. Disintegration did occur, however, by means of transverse cracks which extended from the impact surface to the spall plane and formed a spoke-like pattern on the external impact surface of the specimen (Figure 42). The pattern of these cracks implies that they formed under hoop stresses and the fact that cracks were not found in the free-surface half of the specimen, Figure 43 suggests that these hoop stresses existed only in the impact half of the specimen.

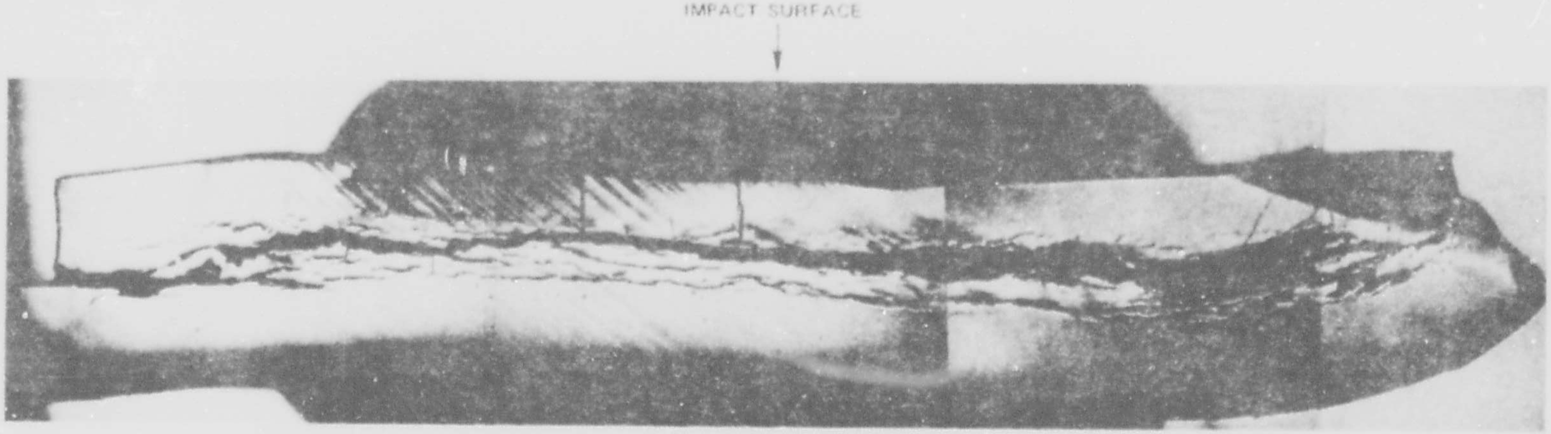

FIGURE 40 POLISHED SECTION THROUGH POLYCARBONATE SPECIMEN NO 12 SHOWING EXTENSIVE DAMAGE CAUSED BY A STRESS LEVEL TWICE THAT REQUIRED TO INITIATE FRACTURE

MP-1033-37

FIGURE 41 PARTIALLY RECONSTRUCTED POLYIMIDE SPECIMEN SHOWING HOW FRAGMENTATION RESULTED FROM CRACK COALESCENCE

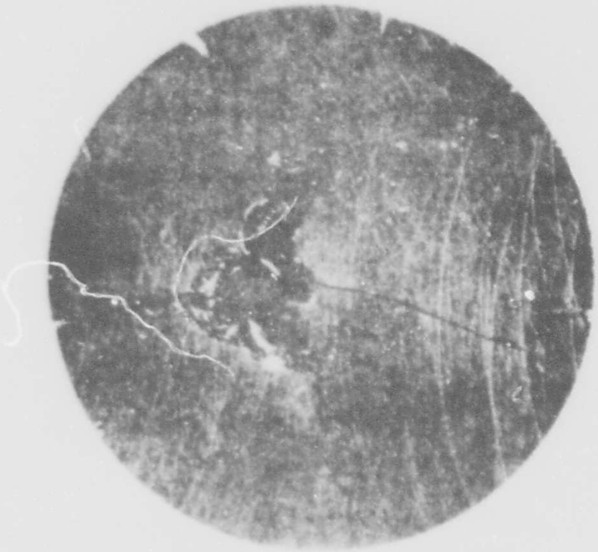

FIGURE 42a RADIAL CRACKS ON THE IMPACTION SIDE OF A POLYIMIDE SPECIMEN CONTRIBUTING TO THE FRAGMENTATION PROCESS

MP-1033-27

FIGURE 42b SAME SPECIMEN WITH A LARGE SECTION REMOVED TO REVEAL INTERNAL DAMAGE

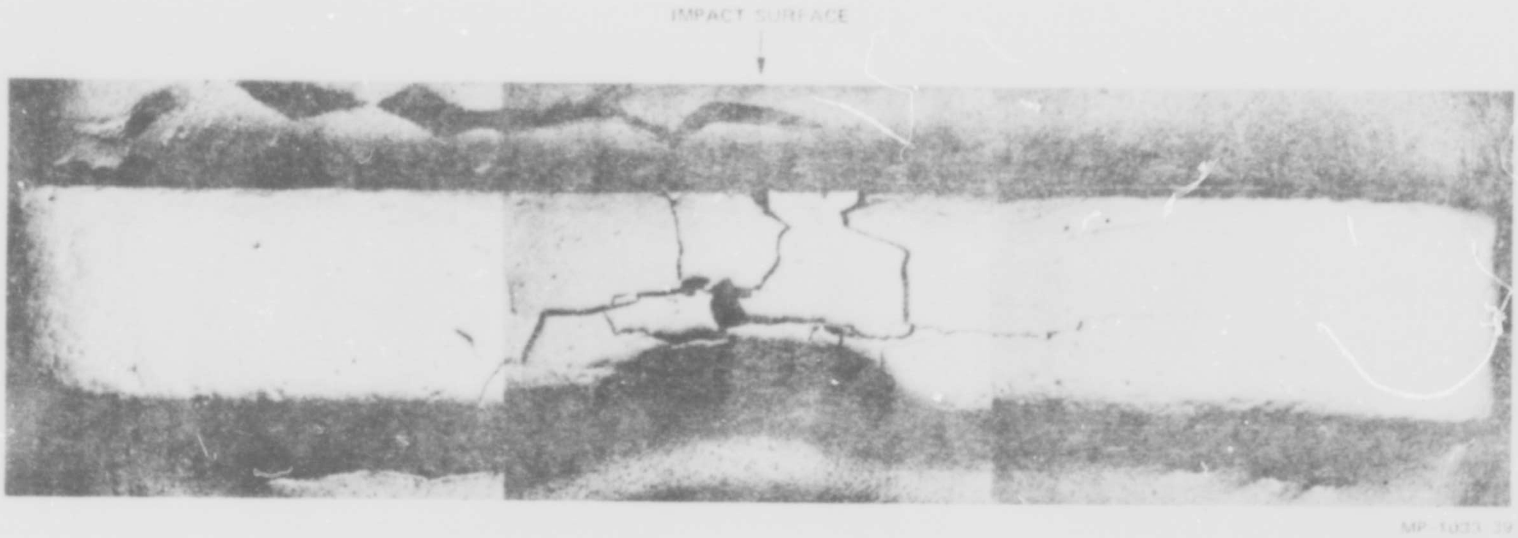

FIGURE 43 POLISHED SECTION THROUGH POLYIMIDE SPECIMEN No. 9 SHOWING SHOCK-INDUCED FRACTURE DAMAGE

V APPLICATION OF NAG METHOD TO HEAT SHIELD FRACTURE

Shock damage is extremely important in many heat shield applications because it precedes the structural response. Experiments at SRI[25] have shown that heat shields exposed to simulated radiation loads may appear undamaged under casual observation, but nonetheless have suffered significant loss of structural strength due to the presence of shock damage.

It would be most useful to develop a capability to predict the extent of shock damage to be expected from arbitrary dynamic loading histories, and to relate this damage to the loss of structural strength. For convenience, the results could be presented in graphs similar to that shown in Figure 44, where contour lines representing various levels of strength degradation are plotted in peak tensile stress-stress duration space. The degree of strength degradation produced by a given stress pulse is shown quantitatively as well as the fact that this strength loss can also occur, for example, at a lower peak stress of somewhat larger duration. The family of curves could represent different amounts of decrease in ultimate tensile strength, bending modulus, or yield strength.

Such graphs can also be transformed by presently available computational techniques to the form shown in Figure 45. In this figure, the same family of curves representing quantitative loss of structural strength is plotted in coordinates representing the fluence and spectral black body temperature of a nuclear device. (The shape of these curves may be more complicated than shown here.) Graphs like those of Figures 44 and 45 could be used by designers and systems analysts to predict quantitatively the structural damage resulting from arbitrary loading histories.

To construct such graphs, we must first be able to quantize damage at an appropriate level of detail. In Figure 46, we again use the coordinates representing peak tensile stress and stress duration. In this case the family of curves represents quantitative levels of microscopic shock damage. Any of several parameters may be used to describe

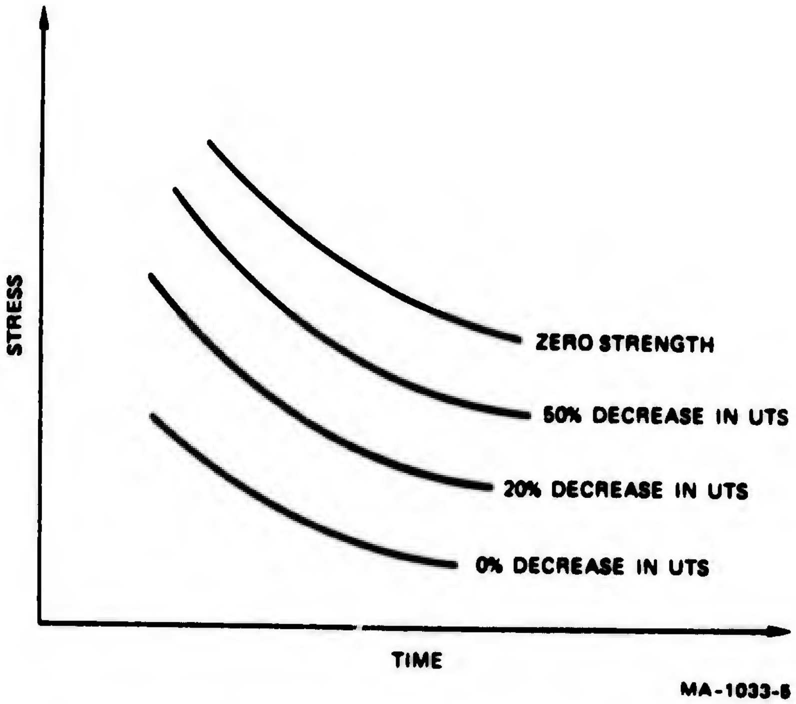

FIGURE 44 STRENGTH DEGRADATION CURVES IN σ - t SPACE

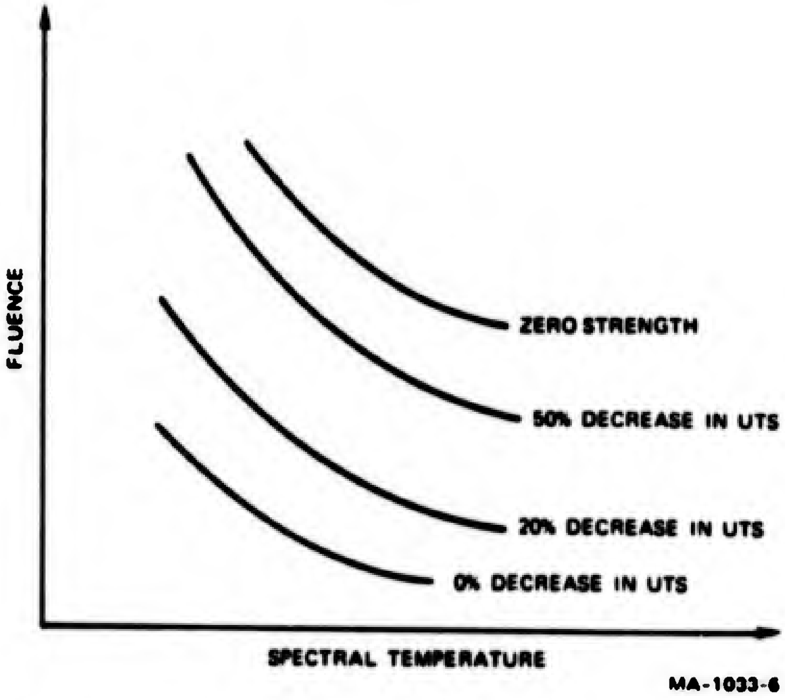

FIGURE 45 STRENGTH DEGRADATION CURVES IN FLUENCE-SPECTRAL TEMPERATURE SPACE

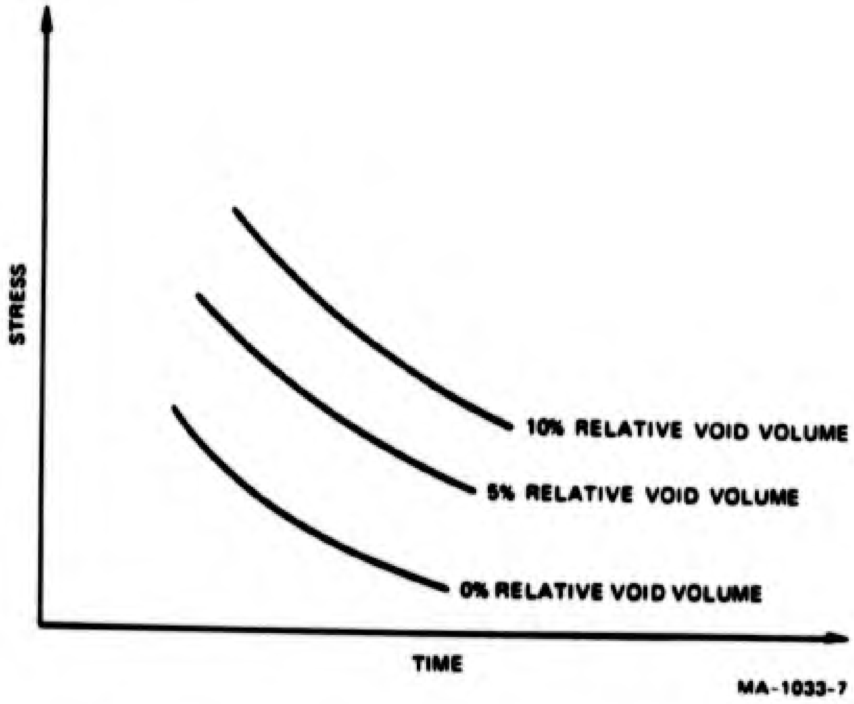

FIGURE 46 QUANTITATIVE ISODAMAGE CURVES

shock damage. In Figure 46 we allow each curve to represent a particular percentage of void volume formed by the microscopic voids or cracks. Another useful damage parameter is void concentration (number of voids per cm^3 of solid material). For a brittle material, crack area may be a more convenient parameter than void volume. Once graphs like Figure 46 are constructed, it should be a straightforward matter to relate experimentally the quantitative damage level curves of Figure 46 to the desired graphs of Figures 44 and 45. Thus, it is clear that our objective must be to provide a capability to construct the curves shown in Figure 46, i.e., curves that will predict the quantitative shock damage distributions caused by arbitrary shock loads.

There have been many previous attempts to characterize shock damage by performing flat-plate impact experiments, but until fairly recently the results were usually presented in the form shown in Figure 47.[26-30]

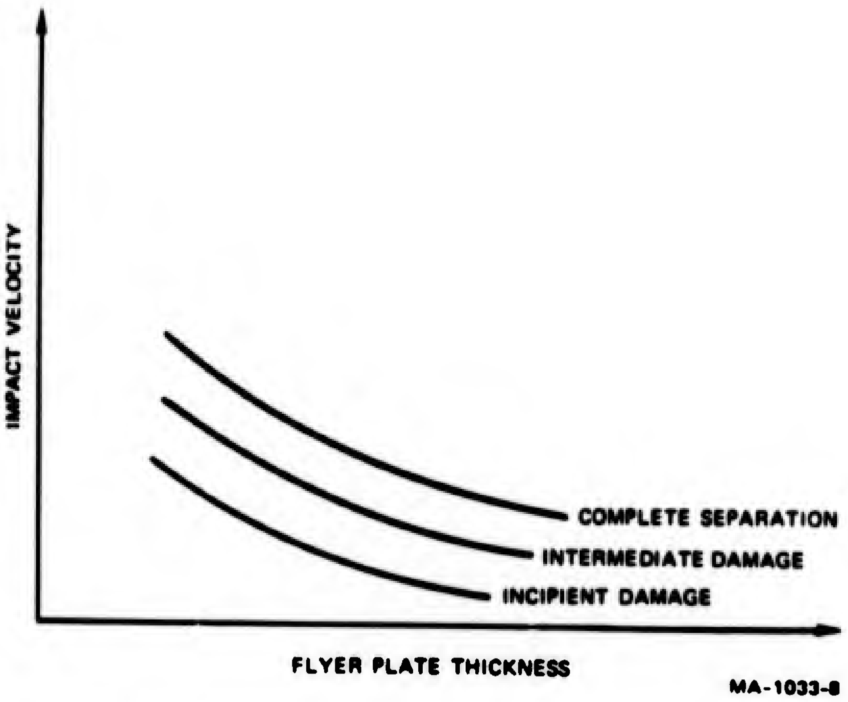

FIGURE 47 QUALITATIVE ISODAMAGE CURVES

In this graph, impact velocity and flyer plate thickness are the coordinates, and the isodamage curves represent vague and qualitative levels of damage such as "cracks visible at 50X," "intermediate damage," and "complete separation." Since impact velocity and flyer plate thickness are related to peak tensile stress and stress duration, respectively, these graphs bear a resemblance to Figure 46. However, it is unclear how to proceed from this type of information to the desired graphs of Figures 44 or 45 for radiation deposition or explosive loading problems. This was the motivation for the development of the NAG method, which was applied in this report to polymers.

VI SUMMARY AND CONCLUSIONS

The incipient fracture behavior of a ductile and a brittle high temperature polymer under shock loading was investigated. Well-controlled flat-plate impact experiments on Lexan polycarbonate and P13N polyimide were carried out using a light gas gun, and a quantitative metallographic technique was used to analyze the damage in each impacted specimen.

The dynamic stress-volume loading and unloading profile for polycarbonate was determined by a gas gun experiment in which multiple electromagnetic particle velocity gages were emplaced in the specimen. Due to the failure of one gage in a similar experiment with polyimide only a rough estimate of these paths could be made for this material.

The constitutive relation data of polycarbonate were used to calculate the approximate stress histories experienced by the specimens, and the damage was correlated with the stress histories to obtain the crack nucleation and growth parameters given in Table VI. The results are also presented in Figure 26 as isodamage contours in stress-stress duration space. Nucleation and growth parameters have lesser meaning for polyimide, which cannot suffer extensive fracture damage and still remain intact. Isodamage contours for this material reduce to a narrow band. For a load duration of about one microsecond, the threshold stresses were determined to be 1.6 kbar for polycarbonate and about 1 kbar for polyimide, and the fracture toughnesses under these dynamic uniaxial strain conditions were estimated to be roughly 60 and 30 $kg/cm^{3/2}$, respectively.

Examination of the virgin material, the compaction heads, and the fracture surfaces of damaged specimens by optical and scanning electron microscopy yielded valuable information about the fracture process, and a fracture mechanism based on these observations was proposed. Essentially two types of microscopic defects were present in the as-received polycarbonate; namely, (1) irregular, two-dimensional flaws and inclusions having an average diameter of about 20 μ and (2) small, spherical, bubble-like voids roughly one micron in diameter. The initial defect structure of polyimide, although not so easily determined, is thought to be similar. Precompression resulting from the passage of the initial compressive wave appeared to have no significant effect on the microstructure and was thus assumed to have no influence on the fracture behavior. Based on observations of the fracture surfaces, fracture in polymers under shock loading is thought to occur by the following mechanism:

1. Activation of a large number of preexisting defects--The larger type of defect, because of its size and sharper edges, can be activated at lower stresses than can the bubble-like flaws, and hence is expected to control this phase of the fracture process at low stresses. At much higher stresses, where the bubble-like defects can also be activated, the bubbles, by reason of their higher density, should be controlling.

2. Radial growth of the activated flaws on planes normal to the impact direction--Propagation occurs slowly at first but, upon reaching a certain size, the crack accelerates more rapidly to constant maximum velocity approaching the speed of Rayleigh waves. The cracks stop abruptly when the stress falls to zero, but may repropagate under subsequent tensile reverberations.

3. Coalescence of expanding cracks--Cracks expanding on parallel planes and approaching one another tend to turn into each other because of the change in stress state at the crack tips when the stress fields interact. The damage at this stage consists of a population of dish-shaped cracks instead of the penny-shaped cracks of stage two.

Coalescence occurs when converging crack tips actually unite with the fracture surfaces of neighboring cracks.

4. Separation of the specimen into two or more parts--This final stage of fracture is reached when individual coalescence events produce one or more continuous fracture paths through the specimen. The large difference between polycarbonate and polyimide in ability to remain intact while suffering damage reflects their relative resistance to crack coalescence. In polyimide, cracks grow together in a brittle manner with very little stress relaxation, whereas the ligaments of material between neighboring cracks in polycarbonate undergo enormous amounts of plastic deformation, thus arresting crack motion, inhibiting coalescence, and preventing separation.

ACKNOWLEDGMENTS

The authors gratefully acknowledge the contributions of their colleagues to this work. In particular, a great debt of thanks is due to Dr. L. Seaman who handled the computational aspects and provided valuable consultation, to T. W. Barbee, Jr., who originated this work and followed the progress with interest, to P. S. DeCarli who performed the static high pressure experiments, to D. Petro for skillful metallographic work, and to Mrs. Bonita Lew for her help in reducing the data.

Thanks are also due to Mr. B. F. Landrun of Geigy Industrial Chemicals for providing the polyimide specimen material, and to Mr. D. W. Caird of General Electric Company for a preprint of his paper, "Maximizing LEXAN Performance," and for information concerning the properties of Lexan.

REFERENCES

1. Barbee, T., Seaman, L., and Crewdson, R. C., Dynamic Fracture Criteria of Homogeneous Materials, AFWL-TR-70-99, Air Force Weapons Laboratory, Kirtland AFB, Albuquerque, New Mexico, November 1970.
2. Barbee, T., Seaman, L., and Curran, D. R., Dynamic Fracture Criteria of Homogeneous Materials, AFWL-TR-71-156, Air Force Weapons Laboratory, Kirtland AFB, Albuquerque, New Mexico, December 1971.
3. Barker, L. M. and Hollenbach, R. E., "Shock-Wave Studies of PMMA, Fused Silica, and Sapphire," J. Appl. Phys. 41, 4208-4226 (1970).
4. Fowles, G. R. and R. F. Williams, "Plane Stress Wave Propagation in Solids," J. Appl. Phys. 41, 360-363 (1970).
5. Cowperthwaite, M. and R. F. Williams, "Determination of Constitutive Relationships with Multiple Gages in Nondivergent Waves," J. Appl. Phys. 42, 456-462 (1971).
6. D. D. Keough, Pressure Transducer for Measuring Shock Wave Profiles, Phase IX, Additional Gage Development, SRI Final Report DASA Contract No. DA-49-146-XZ-096, November 1964.
7. K. W. Schuler, "Propagation of Steady Shock Waves in Polymethyl Methacrylate," J. Mech. Phys. of Solids 18, 277-293, (August 1970).
8. G. M. Bartenev and Yu. V. Zelenev, "Viscoelastic Behavior and Structure of Polymers," Mater. Sci. Eng. 2, 137-156 (1967).
9. Yannas, I. V. and V. C. Haskell, "Utility of the Green-Rivlin Theory in Polymer Mechanics," J. Appl. Phys. 42, 610-613 (1971).
10. Seaman, L., SRI PUFF 3 Computer Code for Stress Wave Propagation, Technical Report No. AFWL-TR-70-51, Air Force Weapons Laboratory, Kirtland AFB, New Mexico, September 1970.
11. Zhurkov, S. N., "Kinetic Concept of the Strength of Solids," Int. J. Fract. Mech. 1, 311 (1965).

12. Dulaney, E. N. and W. F. Brace, "Velocity Behavior of a Growing Crack," J. Appl. Phys. 31, 2233 (1960).

13. Sneddon, I. N., "The Distribution of Stress in the Neighborhood of a Crack in an Elastic Solid," Proc. Roy. Soc. London, A-187 (1946).

14. Irwin, G. R., "Fracture, "Handbuch der Physik VI, ed. S. Flügge, Springer Verlag, Berlin-Göttingen-Heidelberg, 1958, p. 551.

15. Mackenzie, J. K., "The Elastic Constants of a Solid Containing Spherical Holes," Proc. Phys. Soc. B, 63, 2 (1950).

16. Wolock, I. and S. B. Newman, "Fracture Topography," Chap. IIC in Fracture Processes in Polymeric Solids, ed. B. Rosen, Interscience Publishers, New York, London, and Sydney, 1964.

17. Smekal, A., Ergeb. Exakt. Naturw., 15, 173 (1936). (in German)

18. Sommer, E., Ph.D. Dissertation, Ernst-Mach-Institut, Freiburg in Breisgau, Germany (1966). (in German)

19. Berry, J. P., "Brittle Behavior of Polymeric Solids," Chap. IIB in Fracture Processes in Polymeric Solids, ed. B. Rosen, Interscience Publishers, New York, London, and Sydney, 1964.

20. Irwin, G. R., NRL Report 4763, Naval Research Laboratory, Wash. D. C., (1956).

21. Döll, W., Masters Thesis, Scientific Report 3167, Ernst-Mach-Institut, Freiburg in Breisgau, Germany (1967).

22. Terao, N., "Relation between Resistance to Rupture and Mirror Surface of Glass," J. Phys. Soc. Jap. 8, 545-9 (1953).

23. Shand, E. B., "Breaking Strength of Glass Determined from Dimensions of Fracture Mirrors," J. Amer. Ceram. Soc. 42 (10), 474-77 (1959).

24. Irwin, G. R., "Fracture Dynamics," Fracturing of Metals, Amer. Soc. Metals, Cleveland, Ohio, 1948, 147-166.

25. Sliter, G., Colten, J., Romander, C., and Lindberg, H., Characterization of Structural Response for ABM Kill of Reentry Vehicles, Defense Nuclear Agency Contract DASA01-71-C-0006 (1971).

26. Tetelman, A. S. and McEvily, Jr., A. J., Fracture of Structural Materials, John Wiley, New York, 1967, p 40.

27. Charest, J. A., Horne, D. E., and Jenrette, B. D., "Phenomenological Considerations on Spall Measurements," APS Bulletin, 14, 1170 (1969).

28. Butcher, B. M., Spallation of 6061-T6 Aluminum: Behavior of Dense Media Under High Dynamic Pressure, Gordon and Breach, New York, 1968, p 245.

29. Smith, J. H., "Three Low Pressure Spall Thresholds in Copper," Symposium on Dynamic Behavior of Materials, ASTM, Philadelphia, 1963, p 264.

30. Warnicka, R. L., Spallation Thresholds of S-200 Beryllium, ATJ-S Graphite and Isotropic Boron Nitride at 75°F, 500°F, and 1000°F, MSC-68-18, Materials and Structures Laboratory, General Motors Corporation, Detroit, Mich., July 1968.